# Microbially Induced Carbonate Precipitation (MICP) for Seepage-Induced Internal Erosion Control in Sand-Clay Mixtures

**Ning-Jun Jiang** [1*], S.M.ASCE, **Kenichi Soga**, PhD [2], M.ASCE, **Matthew Kuo**, PhD [3]

**Abstract:** Earth embankment dams are one of the most commonly constructed hydraulic infrastructures worldwide. One mode of dam failure is piping through the embankment, which is initiated by internal erosion of soil particles inside dams. In this study, the applicability of microbially induced carbonate precipitation (MICP) for internal erosion control is examined in the laboratory using sand-kaolin mixtures of different particle sizes. A series of internal erosion tests are conducted using a newly designed rigid-wall column erosion test apparatus, which allows independent control of MICP treatment. Erosion rate/coefficient, volumetric change and permeability are characterized during the internal erosion process. It is found that MICP treatment facilitates the reduction of erosion and volumetric contraction of sand-clay mixtures investigated in the current study. Carbonate precipitation increases the erosion resistance of sand-clay mixtures by absorbing/coating fine particles directly and bridging the contacts of coarse particles. An improved effectiveness of internal erosion control is observed in the sand-clay mixture having a higher gap ratio. This observation is due to the inherently large porosity, which hosts more carbonate precipitation. The difficulty of bacteria and chemical injection in sand-clay mixtures triggers the flushing of produced calcium carbonate, which reduces the overall carbonate content and MICP treatment efficiency. The spatial distribution of precipitation within the soil is also altered.

[1] PhD candidate, Department of Engineering, University of Cambridge, Trumpington Street, Cambridge, CB2 1PZ, UK. (*Corresponding author). Email: jiangningjun@gmail.com; nj263@cam.ac.uk. PH/FAX: +44-1223-766683.

[2] Professor, Department of Civil and Environmental Engineering, University of California-Berkeley, Berkeley, CA 94720 USA. Email: soga@berkeley.edu

[3] Project engineer, Cathie Associates SA/NV, 1831 Diegem, Belgium. (Previously, Sharjah Fellow, Department of Engineering, University of Cambridge, Cambridge, CB2 1PZ, UK) Email: matthew.y.kuo@gmail.com

## Introduction

Earth embankment dams are one of the most commonly encountered hydraulic infrastructures worldwide. These are often designed with different functional zones to minimize the likelihood of failures. A typical earth embankment dam has an earth core, upstream and downstream granular filters, and upstream and downstream rockfills. The earth core is often constructed using locally available soils, including clay, sand-clay mixtures, sand-silt mixtures, and in some cases, with gravel (Fell et al. 2005). Clay is particularly erodible and is dislodged easily by seepage flow (Shaikh et al. 1988). Differential settlement or hydraulic fracturing often induces transverse cracks within the impervious dam cores, creating preferential flow pathways through inside the dam cores (Arulanandan and Perry 1983). If the downstream granular filters are inappropriately designed and constructed, the interface between the earth core and downstream filter is likely to be damaged, resulting in the formation of unprotected exits for seepage flow (Fell et al., 2005). Eroded clay may be transported through such unprotected exits. This process typically works its way backward to the upstream side of the dam until a through-piping forms (Bendahmane et al. 2008). It has been reported that piping (which is initiated by internal erosion of soil particles) is the second most frequent failure mode of earth dams after overtopping and accounts for around 46% of all dam failures (Foster et al., 2000). It is therefore of importance to develop engineering countermeasures to prevent piping and internal erosion.

The understanding of seepage-induced soil internal erosion phenomena relies on laboratory experiments (e.g. Fannin and Slangen 2014). Early experimental studies focused on the effect of particle size distribution on internal erosion (Kenney and Lau 1985; Lafleur et al. 1989; Tomlinson and Vaid 2000; Foster and Fell 2001; Wan and Fell 2008). The significance of hydraulic-dependent erosional responses was later recognized, and the hydro-mechanical coupling phenomena in internal erosion processes were extensively investigated. Skempton and Brogan (1994) correlated the critical hydraulic gradients with various particle size distributions to identify the initiation of piping. Moffat et al. (2011) qualitatively observed the spatial and temporal migration of fine particles, and quantitatively measured the axial displacement of tested soils under increased hydraulic gradient by using a large-scale rigid-wall permeameter. Chang and Zhang (2013a) developed a triaxial erosion test device to examine the effect of stress state on the hydraulic gradient that initiates internal erosion. Ke and Takahashi (2012, 2014) experimentally established the relationships between erosion weight, permeability evolution and soil deformation under both rigid-wall and triaxial cell conditions. Based on these experimental studies, it has been widely recognized that the potential for internal erosion depends on the geometric constraints of soils (e.g. particle size distribution and fines content). On the other hand, erosion initiation is determined by hydro-mechanical conditions within soils (e.g. imposed hydraulic gradient, effective stress, and soil density). More recently, Fannin and Slangen (2014) summarised that the distinction of internal erosion phenomena relied on three variables: (i) mass loss, (ii) volumetric change and (iii) permeability change. These previous studies indicate that any erosion mitigation methods should target the modification of soil geometric and/or control of hydro-mechanical conditions in the soil.

There have been several internal erosion mitigation methods proposed and implemented in recent years. These include chemical stabilization (Indraratna et al. 2008; Adams et al. 2013) and seepage flow control/reduction (Fell et al. 2015; Engemoen 2012). Though these methods are able to reduce internal erosion effectively in certain conditions, they still experience problems such as having a failure to appropriately control permeability (chemical stabilization) and requiring large excavation and installation workload (seepage control and reduction). For example, Fell et al. (2005) noted that the installation of protective filter drains and slurry trenches in existing earth dams for erosion and seepage control inevitably involved substantial construction effort.

Microbially induced carbonate precipitation (MICP), a bacteria-induced bio-mineralization process, has been investigated extensively in civil, environmental and infrastructure engineering applications (van Paassen et al. 2010; Cuthbert et al. 2013; DeJong and Montoya 2013; DeJong et al. 2013; Jiang and Soga 2014; Jiang et al. 2014; Montoya et al. 2013; Al Qabany and Soga 2013; Chen et al. 2016; Phillips et al. 2016). The urea hydrolysis by indigenous or exotic urease-producing bacteria (e.g., *S. pasteurii* and *B. megaterium*) is one of the most commonly pathways for bio-mediated carbonate precipitation (Cheng et al. 2014; Soon et al. 2014). The carbonate precipitation via ureolysis involves several stages: synthesis of enzyme through bacteria metabolic activities (Krajewska 2009); catalysis of ureolytic reactions by enzyme and massive production of ammonia ($NH_3$) and dissolved inorganic carbon (DIC) (Eq. 1); alkalinity accumulation at the proximity of bacteria cells (Eqs. 2 and 3); formation of carbonate precipitation on nucleation sites (i.e. bacteria cell surfaces) in the presence of available calcium source (Eq. 4) (Ferris et al. 2004).

$$(NH_2)_2CO + H_2O \rightarrow 2NH_3 + CO_2 \qquad (1)$$

$$2NH_3 + 2H_2O \leftrightarrow 2NH_4^+ + 2OH^- \qquad (2)$$

$$CO_2 + 2OH^- \leftrightarrow HCO_3^- + OH^- \leftrightarrow CO_3^{2-} + H_2O \quad (3)$$

$$Ca^{2+} + CO_3^{2-} \leftrightarrow CaCO_3\ (s) \qquad (4)$$

The produced carbonate precipitation preferentially accumulates at particle-particle contacts (Al Qabany et al. 2012), which is primarily attributed to the microbe's natural preference to avoid exposed particle surfaces, and remain close to smaller surface features (DeJong et al. 2010). Therefore, carbonate precipitation contributes to additional cementation at particle-particle contacts (pore throat). Because of this preference of cementation at pore throat locations, large pores are kept relatively open so that the change in permeability is rather small even though the cementation enhances the soil stiffness (Whiffin et al. 2007; Dawoud et al. 2014a). This is an attractive feature of the MICP technique for internal erosion control. Based on previous studies, the MICP technique gives at least the following highlighted features: (1) Enhancing soil strength and stiffness (Montoya et al. 2013; Al Qabany and Soga 2013); (2) Retaining soil permeability at small calcium carbonate precipitation content (usually smaller than 5-6%) (Martinez et al. 2013; Whiffin et al. 2007; Dawoud et al. 2014a); (3) energy-efficient treatment in the field compared to conventional chemical grouting (DeJong et al. 2014; Dawoud et al. 2014b; Gomez et al. 2015); (4) Fast bio-geochemical reaction rate (Martin et al. 2012; Jiang et al. 2016).

It should be noted that clogging may form in the treated soils, especially at high levels of carbonate precipitation. Feng and Montoya (2016) observed significant heterogeneous precipitation distribution when the soil was heavily-cemented by carbonate precipitation (above 3.5%). Lin et al. (2016) also reported that a carbonate content as low as 1.6% already induced substantial non-uniformity of calcite distribution within the treated soil.

Previous research indicates that effective MICP treatment distances range from 0.2 - 1.0 m (Cuthbert et al. 2013; DeJong et al. 2014; Gomez et al. 2015), due to local clogging. These distances are smaller than what conventional chemical grouting is normally able to achieve (Flora et al. 2013). However, in order to achieve a satisfactory treatment distance, conventional chemical grouting methods usually require substantial energy to inject or mix binders into the soil. This observation is attributed to the high viscosity of the injected conventional binder slurry, especially under high cement-water ratios (Flora et al. 2013). In contrast, the injection of low-viscosity bacteria and cementation solutions can potentially avoid this problem.

Given the aforementioned benefits, the MICP technique can be used to bond fine soil particles (predominantly clay) with coarse fractions in dam cores and consequently, reduce their potential for erosion under seepage flow. Meanwhile, since the MICP technique has the potential to retain existing soil permeability, substantial changes in pore pressure in upstream and downstream zones are avoided, which benefits the structural stability of the dam as a whole. In practice, the MICP technique can be used during the construction of new dams, where bacteria and cementation solutions are mixed with the core fill materials. MICP technique can be also used for emergency remediation of existing dams, where bacteria and cementation agents are injected into the dam cores to reduce ongoing piping/internal erosion. The current study only focuses on the internal erosion control within built dams. The injection method is effective for built dams, since the amount of injected bacteria and cementation solutions is adjustable. Moreover, the injection method facilitates the application of MICP at critical locations based on field situations.

In this study, the MICP technique was tested for internal erosion control in sand-clay mixtures. A series of internal erosion tests were conducted using a newly designed rigid-wall column erosion test apparatus, which allowed independent control of MICP treatment. The progression of internal erosion in three different sand-clay mixtures with/without MICP treatment was examined under increased hydraulic flow rate. Erosion rate/coefficient, volumetric contraction and permeability were monitored during the entire internal erosion test. Finally, the appraisal of MICP treatment for internal erosion control was interpreted in terms of observed hydro-mechanical coupling responses and carbonate precipitation distributions in treated soils.

## Experimental program and procedure

### *Testing Materials*

*Tested soils*

Liner and core materials in embankment dams and levees are often composed of sand-clay mixtures (Marot et al. 2009). In the current study, sand and kaolin clay were used to create internally unstable mixed soils. Three different British Standard graded sands (Fraction B, C and D, supplied by David Ball Group plc.) were used as the coarse fraction. Two graded kaolin clays (Polwhite$^{TM}$ B and E, supplied by Imerys) served as the fine fraction in the binary mixture. The particle size distributions of the sands, kaolin-clays and their mixtures are shown in **Fig. 1**. The sands and kaolin clays were then mixed in three different combinations as shown in **Table 1**. In all three combinations, the ratio between sand and clay was 4:1 based on dry weight (i.e. fine content is 20%). The notations BB, CB and DE in **Table 1** represent the mixtures of 80% Sand B with 20% Kaolin B, 80% Sand C with 20% Kaolin B, and 80% Sand D with 20% Kaolin E, respectively. The fines content was consistent with Fell et al. (2005), who proposed that at least 15% particles passing 0.075 mm are needed inside earthfill dams to achieve the required low permeability. This relatively low fines content (i.e., 20%) also aided the injection of bacteria into soil, as the MICP technique is not effective in clayey soils due to the geometrical constraint for bacteria (Rebata-Landa and Santamarina 2006). The binary mixtures were categorized as gap-graded soils based on the criteria proposed by Lafleur et al (1989). The gap ratio, which is defined as the ratio of the minimum particle size of the coarse fraction and the maximum particle size of the fine fraction in the particle size distribution curve (Chang and Zhang 2013b), was calculated for each sand-clay mixture. Based on the stability criterion for gap-graded soil with fine particles (Chang and Zhang 2013b), the three mixed soils used in this study were deemed to be internally unstable, and were therefore susceptible to seepage-induced internal erosion. BB was the most unstable mixture as it had the largest gap ratio.

*Bacteria and cementation solutions for MICP treatment*

The urease-active strain used in this study was *Sporosarcina pasteurii* (ATCC 6452). This strain was chosen as its urease-synthesis behaviour has been well-defined, and its ureolytic activity has been demonstrated to be higher than many other alternative species (Hata et al. 2013; Seagren and Aydilek 2010). This bacterium strain was cultivated under a sterile aerobic batch condition in the $NH_4$-YE medium (20 g/L yeast extract, 10 g/L $(NH_4)_2SO_4$, and 20 g/L agar in 0.13 M Tris buffer in pH 9.0). After 24 hours incubation at 30 °C, the culture was harvested and stored at 4 °C. Before MICP treatment, bacteria colonies extracted from the $NH_4$-YE medium were introduced into in a urea-rich $NH_4$-YE solution medium (without agar, with an extra 0.5 M urea) and placed in a shaking incubator for 24 hours. This ensured that the final solution contained live bacteria for use in the MICP treatment. The average optical density at 600 nm ($OD_{600}$) of the final solution was 0.22, which was lower than those reported in some previous studies (Al Qabany and Soga 2013). The purpose of using low initial bacteria concentration was to facilitate the injection into the sand-clay mixtures and avoid clogging. The average specific urease activity of the final solution was 2.08 mM $min^{-1}$ $OD^{-1}$, which was sufficient to induce ureolytic reactions (Whiffin, 2004).

The cementation solution used in this study comprised 1.0 M urea, 1.0 M calcium chloride ($CaCl_2$), and 3 g/L nutrient broth, which was consistent with several previous studies that showed effective MICP treatment (Cheng et al., 2013; Al Qabany and Soga, 2013).

***Testing apparatus***

A rigid-wall column erosion test apparatus, which allowed independent control of the MICP treatment, was used to conduct the internal erosion tests in this study (Jiang and Soga, 2014). A schematic diagram of the test apparatus is shown in **Fig. 2**. This apparatus consisted of a rigid-wall column chamber, an upper water reservoir, a peristaltic pump, a pressure indicator, a turbidity meter with data acquisition system, and a collection flask.

The rigid-wall column chamber was composed of a hollow Plexiglas column with a height of 140 mm and inner diameter of 50 mm. The column was mounted with top and bottom plates using four threaded rods. O-rings sealed the gaps between the column and plates. A funnel-shaped draining system was created inside the bottom plate to avoid particle clogging. A steel perforated plate with an opening size of 1 mm was installed between the column chamber and the bottom plate. On top of the perforated plate, a nylon filter with an opening size of 100 μm was placed, which only permitted clay particles to pass through. The peristaltic pump was used in a flow-rate-controlled mode to provide a maximum flow rate of 40 mL/min. The turbidity meter (Analytic Technology Inc.) was installed to obtain clay particle concentrations in the outlet effluent solution through optical transmittance measurement (Haghighi et al. 2013). A calibration was made prior to the erosion test to correlate the optical signal received by the data acquisition system with the clay concentration in the solution (in an increment of 0.05 mg/L).

It should be noted that it is an inherent limitation of the rigid-wall column chamber apparatus that preferential flow may form at soil-wall boundaries at high flow velocities, due to larger pore spaces at the boundary than inside the soil matrix. In terms of the internal erosion test, the erosion observed at the boundary is expected to be greater than inside the soil matrix. In the current study, however, the substantial amount of clay particles in soil matrix may mitigate the preferential flow at soil-wall boundaries, as suggested by Daniel et al. (1985).

## ***Testing methods***

### *Specimen preparation*

Dry sand and kaolin-clay were first mixed thoroughly before being air-pluviated into the column chamber to achieve the fines content of 20%. Mixed soils were then statically compacted in three layers to achieve a final height of 100 mm and a dry density of 1.53 g/cm$^3$. Particle size distribution analysis was conducted after the dry-tamping and confirmed the uniformity of the sand-clay mixtures with respect to specimen depth. A nylon filter was then placed on top of the sand-clay mixtures with the headspace filled with gravel, which served as a water diffuser during the erosion test. Finally, the column chamber was sealed and a $CO_2$-aided saturation method was used to reduce the saturation time of the sand-clay mixtures without disturbing their initial states (Xiao and Shwiyhat 2012).

*MICP treatment*

The MICP treatment was divided into two stages: (1) bacteria solution injection, and (2) cementation solution injection. A schematic illustration of the MICP treatment procedure is shown in **Fig. 3**. Three different injection strategies (M1, M2 and M3) were implemented to optimise the MICP treatment for internal erosion control. Optimisation of the MICP process in terms of injection rate and chemical concentration for sandy soils has been undertaken by Al Qabany et al. (2012). It was found that an injection rate of below 0.42 mol/L/h with multi-injection and $CaCl_2$/urea concentration up to 1.0 M resulted in an improved MICP treatment efficiency. Martinez et al. (2013) reported that the injection velocity of 29.7 cm/h and $CaCl_2$ to urea ratio smaller than 1 with stopped-flow injection technique also optimized the MICP process. In the current study, the optimized chemical concentration used by Al Qabany et al. (2012) and the chemical ratio used by Martinez et al. (2013), namely 1.0 M $CaCl_2$ and 1.0 M urea, were adopted. A smaller injection velocity (6.1-12.3 cm/h in terms of sample cross-sectional area) and fewer injection phases than the two previous studies were applied. These experimental conditions were used due to the substantial amount of clay particles in the soil matrix, which would make fast injection difficult to implement.

In M1, the bacteria solution was injected from the top of the saturated sand-clay mixture specimens at 2mL/min (6.1 cm/h in terms of the sample cross-sectional area). The total injection volume was 1.5 pore volume of soil (PV) to ensure all pore spaces were filled with the bacteria solution. The bacteria were then retained in the soil matrix for 12 hours before one phase of 1.5 PV cementation solution was injected in the same manner at 4 mL/min. Finally, the specimens were cured for another 12 hours before subjected to the seepage erosion test.

In M2, the same volumes of bacteria solution and cementation solution were injected at the same flow rate as in M1. Retention time was also the same as in M1. The only difference was that M2 had two phases of 1.5 PV cementation injection with an inter-phase retention time of 10 hours.

In M3, the same injection regime of bacteria solution and cementation solution was used as in M2. But a lower injection rate of 2 mL/min was adopted for cementation injection.

In all three cases, the injection rates for both bacteria and cementation solutions were lower than the minimum flow rate (4.47 mL/min) in the subsequent erosion test to avoid erosion at this stage. For direct comparison, erosion tests were also conducted in untreated samples. It should be noted that the untreated control soil specimens (marked as "U") were subject to the same treatment procedure, but only using distilled water (bacteria and chemicals were not injected).

*Internal erosion test*

Both untreated and MICP treated specimens were subject to flow-rate-controlled internal erosion test. Triple samples were tested to ensure the repeatability of the results. The internal erosion test is schematically shown in **Fig. 4**. The internal erosion test was initiated with a downward flow rate of 4.47 mL/min. The downward flow direction in this study differs from that in the field, which is likely to be parallel to the orientation of the soil lifts. However, this study is only an element-scale test. The prepared sand-clay mixture specimens are viewed as an element within the real dam core and are regarded as isotropic hydraulically and mechanically.

The peristaltic pump was then run at different flow rates for nine consecutive stages while the flow rate was kept constant at each stage. When the erosion concentration reached a steady-state condition, the test then proceeded to the next stage with a higher flow rate. Photos were taken at the start and the end of each stage to facilitate the visual check of onset and progression of internal erosion. Simultaneously, the overall pressure difference, specimen length, time-dependent clay concentration in effluent solution, and pH, Electrical Conductivity (EC) and ammonium concentration (c[$NH_4^+$]) of the effluent solution were monitored during the course of the experiments. Based on these monitoring parameters, the peak erosion rate and accumulative erosion weight, hydraulic shear stress, permeability, and volumetric contraction were obtained.

It should be noted that the flow rate and measured hydraulic gradient in this study were mostly smaller than those reported by Reddi et al. (2000) and Bendahmane et al. (2008). This specification is attributed to the fact that the flow rate provided by the peristaltic pump reduces rapidly under increasing pump tube pressure. Preliminary test showed that hydraulic pressure needs to be kept below 200 kPa (200 m/m) to avoid significant reduction in flow rate. Therefore, small flow rates were selected in this study to maintain relatively low pump tube pressures.

It is also worth mentioning that the flow rate and measured hydraulic gradient were still significantly larger than those encountered in the field ($i \approx 1.0$). Tests under higher hydraulic gradient (flow velocity) were conducted to consider the possible shortened flow path in a dam by backward erosion. In this case, the local gradient is much higher than the global one.

*Monitoring techniques*

The pressure difference along the specimen was obtained via an electronic pressure indicator. The time-dependent kaolin-clay concentration was measured using an ATI turbidity meter at a recording interval of 1s. The specimen length was measured by a calliper at the start and end of each erosion stage. pH and EC of effluent solutions were measured via a Jenway 3510 pH meter and a Mettler Toledo FiveGo conductivity meter, respectively.

$c[NH_4^+]$ in the effluent solution was measured using the modified Nessler method (Whiffin et al. 2007). The solution samples were diluted with deionized water to target a range of 0–0.5 mM. 2 mL diluted solution sample was mixed with 100 μL Nessler reagent in a cuvette and reacted for exactly 1 min. The sample was subject to the optical absorbance measurement using a Visible spectrophotometer at the wavelength of 425 nm. Absorbance readings were then converted to $c[NH_4^+]$ by referring to the calibration curve from $NH_4Cl$ standard solutions.

In the control MICP treated samples that were not subject to erosion process, carbonate precipitation content distributions in soil matrix was measured by using an airtight chamber with a barometer. During the measurement, disaggregated soil samples (using mortar) and chloride acid were initially placed into two compartments in the chamber. The chamber was then enclosed and shaken to thoroughly mix the soil with the acid. Pressure readings in the barometer due to $CO_2$ production were recorded and converted to the corresponding carbonate contents by referring to the calibration curve obtained from $CaCO_3$ standards.

## Results

The results of the internal erosion tests are analysed in terms of: 1) visual observations; 2) erosion characterization 3) hydro-mechanical and chemical responses. Comparisons are made between the untreated and MICP treated soils in terms of the three points.

### *Visual observations*

Visual observation is a useful method to quickly identify the occurrence and progression of internal erosion (Moffat et al. 2011). In this study, photos were taken at every stage of the internal erosion for all samples. Example cases of CB_U (i.e. untreated soil) and CB_M1 are shown in **Fig 5**. Similar erosion patterns were observed in most of the other cases. For both untreated and MICP treated soils, the increased flow rate resulted in more noticeable fine particle erosion along the inner surface of the transparent Plexiglas wall, as marked with dashed red circles. Erosion was also found to be less severe in the MICP treated samples than in the untreated samples under the same flow rate.

***Internal erosion characterization***

The most straightforward indication of internal erosion is the concentration of flushed particles in the downstream flow. **Fig. 6** shows the time-dependent clay concentrations in the effluent of representative samples of CB_U (untreated) and CB_M1 (MICP treated). In both cases, the clay concentrations peaked at a flow volume less than 0.5 PV and then reduced gradually. The clay concentrations became stable when the flow volume was approximately 1-3 PV, depending on flow rate. This time-dependent erosion pattern for the representative samples was confirmed to be consistent for all other samples in this study.

The magnitudes of peak clay concentration in the case of CB_M1 (**Fig. 6b**) were noticeably lower than those in the case of CB_U (**Fig. 6a**) at the flow rate ranging from 4.47 to 25.98 mL/min, inferring that the internal erosion was less severe in MICP treated sand-clay mixtures. At higher flow rates, the peak clay concentration in the case of CB_U dropped below 0.50 mg/L due to clogging at the near-bottom-mesh part.

The peak erosion rate, which is the maximum erosion weight per unit time per unit cross-section area, has been used extensively as an indication of soil erosion (Bendahmane et al. 2008; Marot et al. 2012). As the peak erosion rate is attributed to the initial turbulence, or local vortices (Gruesbeck and Collins 1982), it is considered to be predominantly determined by the current flow condition while the influence of previous flow stage is negligible.

Comparison is made between the untreated and the MICP treated samples in terms of the relationship between peak erosion rate and hydraulic shear stress, as shown in **Fig. 7**. The error bars for both peak erosion rate and shear stress are also plotted. The hydraulic shear stress here is defined after Bendahmane et al. (2008) and Reddi et al. (2000) as:

$$\tau = \frac{\Delta p}{h} \cdot \sqrt{\frac{2k\eta}{\rho_w g n}} \tag{5}$$

where $\Delta p$ is the pressure difference (Pa); $h$ is the specimen height (m); $k$ is the hydraulic conductivity of sand-clay mixture (m/s); $\eta$ is the viscosity of water ($1.005\times10^{-3}$ kg/m s); $\rho_w$ is the density of water (1000 kg/m$^3$); $g$ is the gravity acceleration (9.81 m/s$^2$); $n$ is the porosity of the sand-clay mixture. The calculation of porosity should account for the produced calcium carbonate precipitation. From **Fig. 13**, it can be found that the carbonate contents are only less than 1% of the total weight of soil. Therefore, the weight of carbonate precipitation was ignored when calculating porosity in **Eq. 5**.

The occurrence of particle detachment primarily depends on the shear stress on pore walls through pore-fluid flow. Khilar et al. (1985) and Reddi and Bonala (1997) specified the relationship between erosion rate and hydraulic shear stress from the perspective of particle kinetics as follows:

$$r = \alpha(\tau - \tau_c) \tag{6}$$

where $r$ is the erosion rate (g m$^{-2}$ s$^{-1}$); $\alpha$ is the erosion coefficient ($10^{-3}$ s m$^{-1}$); $\tau$ is the wall or surface shear stress (Pa); $\tau_c$ is the critical hydraulic shear stress (Pa). **Eq. 6** highlights the fact that erosion only occurs when the shear stress is greater than a critical value.

The evaluated values of $\tau_c$ are marked by the dashed circles in **Fig. 7**. In the case of BB soils (**Fig. 7a**), the $\tau_c$ value for untreated soils was only around 0.26 Pa. For MICP treated samples, it was around 0.38 Pa. No distinction was found among different MICP strategies (M1, M2 or M3). In the case of CB and DE soils (**Fig. 7b** and **7c**), however, $\tau_c$ values were almost identical for all samples (0.52 Pa for CB soils and 0.70 Pa for DE soils). The effect of MICP treatment on $\tau_c$ also appeared to be insignificant in the case of CB and DE soils.

Linear fitting was performed between the peak erosion rate and shear stress for the post-critical shear stress stage, as shown in **Fig. 7**. The peak erosion rate and shear stress showed strong linear relations in all cases, generally with $R^2 > 0.95$. The erosion coefficient ($\alpha$) was determined based on the linear correlations, and the results are shown in **Fig. 8**. In the case of the BB soil, the untreated sample had the largest $\alpha$ (= $0.775\times10^{-3}$ s m$^{-1}$), followed by M2 ($0.596\times10^{-3}$ s m$^{-1}$), M3 ($0.360\times10^{-3}$ s m$^{-1}$), and M1 ($0.260\times10^{-3}$ s m$^{-1}$). In the case of the CB soil, the untreated sample also had the largest $\alpha$ (= $0.465\times10^{-3}$ s m$^{-1}$) while $\alpha$ value of the M2 sample ($\alpha_{M2} = 0.303\times10^{-3}$ s m$^{-1}$) was the largest among all MICP strategies ($\alpha_{M1} = 0.285\times10^{-3}$ s m$^{-1}$ and $\alpha_{M3} = 0.234\times10^{-3}$ s m$^{-1}$). The DE soils, however, exhibited different behaviour from the previous two cases. $\alpha_{M2}$ ($1.931\times10^{-3}$ s m$^{-1}$) and $\alpha_{M3}$ ($1.124\times10^{-3}$ s m$^{-1}$) were larger than $\alpha_U$ ($0.684\times10^{-3}$ s m$^{-1}$) while $\alpha_{M1}$ ($0.373\times10^{-3}$ s m$^{-1}$) was the smallest. It should be noted that the untreated soils experienced a significant drop in the peak erosion rate at high shear stresses. This is because that the soil skeleton was significantly disturbed at the high shear stress. Fine particles were quickly dislodged, so that the near-bottom-mesh part of the specimen was clogged, which was also observed by Reddi et al. (2000).

The magnitudes of $\tau_c$ and $\alpha$ in this study are comparable to the results obtained by Reddi et al. (2000) and Bendahmane et al. (2008), as shown in **Fig. 7**. In Reddi et al. (2000), the $\tau_c$ value of 1.23 Pa and $\alpha$ value of $25\times10^{-3}$ s m$^{-1}$ were obtained from 50-mm-high cylindrical sand-clay mixture samples with 30% fine content. The larger value of $\tau_c$ obtained by Reddi et al. (2000) was primarily due to smaller height and porosity of the soil sample. The larger value of $\alpha$ was due to a much larger flow rate (at least one order higher than in the current study) in their internal erosion test. The magnitudes of $\tau_c$ in this study were quite consistent with that reported by Bendahmane et al. (2008) ( i.e., 0.7 Pa) for a sand-kaolinite mixture with 20% fine content.

However, high hydraulic gradient levels, up to 100 m/m used by Bendahmane et al. (2008) resulted in a higher $\alpha$ value (i.e., $3.2\times10^{-3}$ s m$^{-1}$) than those measured in the current study.

No previous studies provide field data for the $\alpha$-$\tau$ relationship. This is attributed to the difficulty in characterizing shear stress in the field, as the shear stress varies at different locations in the dam due to heterogeneity of soil properties and flow regime. Instead, flow discharge and piezometer head are usually monitored, and used as indicators for internal erosion/piping in the field (Flores-Berrones et al. 2011; Danka and Zhang 2015). To facilitate the design of erosion-free dams, the $\alpha$-$\tau$ relationship is usually characterized through standard laboratory element tests such as the hole erosion test (Wan and Fell 2004; Haghighi et al. 2013; Reddi et al. 2000).

***Hydro-mechanical and chemical responses***

Accompanying the loss of fine particles from the sand-clay mixture is an alteration of hydro-mechanical behaviours. In this study, the evolution of volumetric contraction and change in permeability were monitored during internal erosion to examine the hydro-mechanical responses of MICP treated sand-clay mixtures. pH, EC and c[$NH_4^+$] of effluent solution were measured to understand the chemical responses.

*Hydro-mechanical responses*

**Fig. 9** shows the variations of volumetric contraction and permeability with accumulative erosion weight. Volumetric contraction induced by internal erosion is regarded as an adverse mechanical response as it leads to excessive ground settlement. Permeability is a controlling factor for the hydraulic-barrier performance of earth embankment dams. The initial permeability of sand-clay mixtures is presented in **Fig. 9**. The magnitudes of their initial permeability satisfy the seepage control requirement by USSD (2011), which suggests that the maximum permeability of broadly graded core materials is around $10^{-6}$ m/s. From **Fig. 9**, it can be seen that both permeability and volumetric contraction increased steadily with increasing accumulative erosion weight, regardless of sand-clay mixtures and MICP strategies. Based on the conceptual framework proposed by Fannin and Slangen (2014), the observed coupling relationships between erosion weight, volumetric contraction and permeability in this study fit the features of *suffosion*, which means that the loss of fine particles under increased hydraulic gradient also induces disturbance and rearrangement of coarse particle skeleton (Richards and Reddy 2007).

It is also found that the permeability of the untreated soils increased less rapidly with accumulative erosion weight than the MICP treated samples for all three soils. In contrast, the volumetric contraction of the untreated soils increased more rapidly with accumulative erosion weight than the MICP treated samples for all three soils. The volumetric contraction – permeability relations are thereafter presented in **Fig. 10**. Regardless of soil type and MICP treatment strategies, untreated soils had consistently smaller permeability values than the MICP treated samples for a given volumetric contraction.

For untreated soils, fine particles begin migrating and are flushed out under increased hydraulic flow rate. If the volumetric change is not accounted for temporarily, the porosity of untreated soil increases during the process of fines erosion, with an associated increase in permeability. However, volumetric contraction occurs as the coarse skeleton is disturbed. This in turn reduces soil porosity and results in the untreated soils becoming less permeable.

For MICP treated soils, the carbonate precipitation via MICP provides particle-particle contact cementation and improve soil stiffness (Montoya et al. 2013; Al Qabany and Soga 2013), but keeps the pore space open for pore fluid flow. At the same amount of fine particle loss, the higher stiffness of MICP treated soils results in a smaller volumetric contraction than in the untreated soils. The higher stiffness of MICP treated soils also means their permeability tends to be larger than that of the untreated soils (see **Fig. 9**).

It is generally understood that the sand-clay mixtures become more brittle after stiffness enhancement by MICP treatment (Montoya and DeJong 2015). The enhanced stiffness means that the treated soil is more susceptible to crack-forming under differential settlement. Further efforts are needed to quantify the effect of MICP treatment on crack-forming resistance of earth dam cores. On the other hand, the bulk and differential settlements of treated soils are substantially smaller than in untreated soils. The structural stability of earth dams is therefore likely to be improved by the use of MICP treatment.

It should be noted that most previous studies on volumetric contraction during internal erosion focus on cohesionless soil mixtures. To the knowledge of the authors, there are no reported cases that address sand-clay mixtures. The magnitudes of volumetric contraction for untreated sand-clay mixtures in this study are much greater than those reported for cohesionless soils (mostly less than 1%) (Moffat et al. 2011; Xiao and Shwiyhat 2012). This is possibly attributed to the reduced compressibility of cohesionless materials and well-controlled confining pressure in these previous studies.

*Chemical responses*

In order to satisfy regulatory compliance for environmental protection, it is necessary to demonstrate that MICP is an environmentally friendly technique for internal erosion control. In this study, the chemical properties such as pH, EC and c[$NH_4^+$] were monitored during the course of the internal erosion tests. An example from the BB soils is shown in **Fig. 11**, which is representative of the typical pattern of chemical responses observed in this study.

It is found that the effluent of the untreated soils attained stable neutrality with pH fluctuating slightly between 6.9 and 7.3. On the other hand, the effluent pH of BB_M2 soils peaked at 8.5

(2.8 PV) due to the presence of ureolysis-induced alkaline substances in the pore solution. The pH value then steadily reduced to neutrality with continuous water flushing (up to 22 PV). It should be noted that the initial effluent pH value of BB_M2 soils was only 7.4, which is attributed to the mineralogy of the soil matrix. As kaolin clay used in this study had a pH value of 5.0, the sand-clay mixture itself was acidic. This explains the low effluent pH value for BB_M2 soils at the beginning of flushing. With further flushing, the effect of soil mineralogy on effluent pH became insignificant.

The EC of BB_M2 decreased steadily from around $10^5$ μs/cm to less than $10^3$ μs/cm, demonstrating a reduction of electrolytic ions in the pore solution with increased water flushing. Nevertheless, the resulting magnitude of effluent EC for BB_M2 soils was still about 2 orders of magnitude larger than that of BB_U soils. This indicates that large amounts of electrolytic ions from the ureolytic reactions were present in the pore solution prior to the erosion test.

The ammonia concentration c[$NH_4^+$] was initially very high at about $10^4$ mg/L due to the ureolytic reactions. With water flushing, a reducing trend similar to effluent EC was observed and c[$NH_4^+$] decreased to 35 mg/L after 22 PV of water flushing. This value was still above the Aquatic Life Ambient Water Quality Criteria for Ammonia (17 mg/L) (USEPA 2013). Hence, a proper environmental impact assessment is required to ensure that c[$NH_4^+$] is diluted to meet the regulatory requirement.

## Discussion

### *Effect of sand-clay mixture types*

In order to clarify the influence of the sand-clay mixture types on the efficiency of internal erosion control by MICP, the magnitudes of erosion coefficient ($\alpha$), ultimate volumetric contraction and ultimate relative permeability (the ratio between the permeability at later stage and the initial value) of all MICP treated samples are normalized based on corresponding untreated soils. The normalised values are compared against gap ratio, as shown in **Fig. 12.** For soils with large gap ratios or coarse host sands (BB and CB), the $\alpha$ values of the MICP treated soils were reduced by 25% to 75%, compared to the untreated soils. The volumetric contraction of the treated soils was found 20% to 40% of that for untreated soils. These observations contrasted to the results of DE samples, which had a smaller gap ratio and smaller particle sizes. The normalised $\alpha$ values of MICP treated DE soils varied between 0.5 and 2.5, indicating that the treatment was not effective, and sometimes even had an adverse effect in terms of erosion control. The ability of MICP treated DE soils to restrict erosion-induced volume contraction was also limited compared to the MICP treated BB and CB soils. The unsatisfactory performances of MICP treated DE samples are attributed to possible hydraulic fracturing during the bacteria and chemical injection processes, as internal cracks and/or preferential flow paths can be generated by hydraulic fracturing. Actually, the recorded pressure differences during the final chemical injection phase (which created the highest injection pressure) were 12-19 kPa, 34-40 kPa, and 55-80 kPa for BB, CB and DE soils, respectively. The DE soils experienced the highest injection pressure, making it more vulnerable to hydraulic fracturing. Further investigation on this aspect is needed.

The overall carbonate contents in MICP treated BB, CB and DE soils are shown in **Fig. 13**. The values of normalised erosion coefficient are plotted against overall carbonate content in **Fig. 14**. It can be seen that higher levels of carbonate precipitation occurred in the BB and CB samples (0.4-0.6% in weight) than in the DE soils (0.2% in weight). Higher porosity in the soil matrix of BB and CB samples is believed to result in the increased carbonate precipitation content (Fonseva et al. 2014). Consequently, the higher carbonate precipitation content resulted in improved erosion resistance in BB and CB soils. From **Fig. 14,** it can be found that the erosion coefficient is significantly reduced at higher carbonate content. Fundamentally, produced carbonate precipitation mitigates internal erosion in two ways: (i) absorbing and/or coating fine particles directly due to its high surface area (Al-Thawadi 2012); and (ii) bridging the contacts of coarse particles to increase soil stiffness (Cheng et al. 2013). The former mechanism contributes to a smaller amount of fines loss, and the latter mechanism results in the treated soils being less susceptible to volumetric contraction. An increased amount of carbonate therefore needs to be precipitated to provide improved erosion resistance for the DE soils.

It is found that the overall carbonate contents measured in this study are smaller compared with similar studies using 1.0 M chemical solutions (Whiffin et al. 2007). This is likely to be attributed to: (i) fewer chemical injections, (ii) smaller host soil matrix (reduced porosity), and (iii) injection-induced carbonate precipitation flushing.

The efficiency of MICP treatment in this study is shown in **Fig. 13**. It is defined as percentage ratio of chemical amount between the measured calcium carbonate after MICP treatment and injected calcium chloride (Al Qabany et al. 2012). It is observed that the treatment efficiencies for M1, M2 and M3 were less than 10%, which were significantly less than those reported in pure sand or other coarser granular soils (Al Qabany et al. 2012; Martinez et al. 2013). This observation indicates that 1.0 M of chemical concentration is greater than the optimized concentration for the sand-clay mixtures when $OD_{600}$ equals to 0.22. In addition, finer host sand (relatively smaller porosity) is found to correspond to lower MICP treatment efficiency.

The carbonate distribution with respect to specimen depth is presented in **Fig. 15**. It is found that carbonate precipitation was preferentially distributed over the upper part of the BB soils. However, in the CB and DE soils, increased carbonate precipitation was observed over the lower half of the treated soils. As the BB soil had higher porosity, the formed carbonate precipitation was subject to less downward hydraulic pressure during MICP treatment so that they stayed where they were produced. In CB and DE soils, the generated downward pressure during cementation injection was much higher due to smaller porosity of soil matrix. Consequently, produced carbonate precipitation was flushed downwards, which resulted in an accumulation of carbonate precipitation at the lower half of soil.

### *Effect of MICP treatments*

In this study, M1 and M2 had the same injection rate, while M2 had one additional chemical injection. M2 and M3 had the same number of injections, but the injection rate in M2 was twice that of M3. These differences resulted in varied erosional behaviours of soils subject to different MICP treatment strategies. More specifically, the M1 soils had a smaller erosion coefficient than the M2 soils (see **Fig. 12**), regardless of soil mixtures. The erosion coefficients of the M2 soils were also higher than the M3 soils, independent of soil mixtures.

Comparing overall carbonate precipitation content produced by M1 and M2, it can be observed that higher levels of calcium carbonate was presented in M1 than M2 regardless of soil mixtures (see **Fig. 13**). As M1 and M2 had the same injection rate for the bacteria and first chemical injections, it is concluded that the further chemical injection in M2 resulted in the loss of carbonate precipitation. If the results of M2 are compared with M3, it can be seen that the carbonate precipitation was larger in M3 than in M2 regardless of soil mixtures (see **Fig. 13**). As M2 and M3 had the same number of injections, the lower injection rate in M3 contributed to reduced calcium carbonate flushing. In terms of the efficiency of MICP treatment, M1 had the highest efficiency among the three strategies. The M2 and M3 soils had lower efficiency of MICP treatment due to the injection-induced flushing of calcium carbonate precipitation.

## Conclusions

This paper presents the results of a laboratory investigation on MICP for internal erosion control in sandy-clay mixtures. Soil samples were subject to different flow rates to monitor the erosional, hydro-mechanical and chemical responses when internal erosion was taking place. The following conclusions are drawn from the experimental results:

(1) The MICP treatment contributed to an enhanced critical shear stress and a reduced erosion coefficient for sand-clay mixtures with a large gap ratio (using coarser host sand) when subject to a constant flow rate erosion test. However, the improvement in critical shear stress and erosion resistance was insignificant for a mixed soil with a small gap ratio (finer host sand) due to its inefficiency in carbonate precipitation during the MICP treatment phase.

(2) The tested sand-clay mixtures exhibited steady increase in permeability and volumetric contraction with increasing accumulative erosion weight. An erosion mode of *suffosion* was identified for the sand-clay mixtures. Regardless of the gap ratio of the tested soils, the MICP treatment resulted in the sand-clay mixtures exhibiting reduced volumetric contraction when fines were eroded.

(3) The effectiveness of MICP for internal erosion control was mainly dominated by the amount of produced carbonate precipitation, which absorbed/coated fine particles directly and bridged the contacts of coarse particles. Sand-clay mixtures with a large gap ratio were able to produce increased levels of precipitated carbonate, which corresponded to reduced fines loss and smaller volumetric contraction.

(4) The difficulty with injecting bacteria and chemical solutions into sand-clay mixtures caused the flushing of produced calcium carbonate. The precipitation flushing reduced the overall carbonate precipitation content and MICP treatment efficiency. The spatial distribution of calcium carbonate in the sand-clay mixtures was also modified.

The analysis of erosional and hydro-mechanical responses during the internal erosion process is of importance in providing practical guidance for potential future field trials of MICP. Results from this study show that soil properties such as particle size distribution, fine particle content and gap ratio are important in determining whether MICP is feasible for internal erosion control. If MICP is implemented in the field, the content and spatial uniformity of carbonate precipitation need to be ensured in order to achieve improved control effectiveness. This research has the following limitations: (1) only one fines content was tested and the performance of MICP treatment has not yet been validated in soils with different fines content; (2) the use of the rigid-wall column chamber made the control of confining pressure difficult, and potential leakage problems may exist at the boundary between soil and the rigid-wall at high seepage velocities; (3) the downward direction of seepage flow in the tests differs from the flow conditions in real dams, and the hydraulic pressure/gradients in the tests are significantly larger than those encountered in the field; and (4) non-destructive monitoring techniques can be adopted to observe the interaction between carbonate precipitation and sand-clay mixtures. In the future, further studies need to be conducted to address these problems.

## Acknowledgements

The authors thank Mr. Knight Chris for manufacturing the experimental device. Special thanks are also extended to Mr. Osama Dawoud and Dr. Fei Jin for their involvements in result analysis and discussion. Advice from Prof Arkihiro Takahashi and Dr. Ke Lin from Tokyo Institute of Technology is also greatly appreciated. The first author also extends thanks to China Scholarship Council (CSC) and Cambridge Commonwealth, European & International Trust for their financial support in the PhD studentship.

## Reference

Adams, B. T., Xiao, M., and Wright, A. (2013). "Erosion mechanisms of organic soil and bioabatement of piping erosion of sand." *J. Geotech. Geoenviron. Eng.*, 139(8), 1360–1368.

Al Qabany, A., and Soga, K. (2013). "Effect of chemical treatment used in MICP on engineering properties of cemented soils." *Géotechnique*, 63(4), 331–339.

Al Qabany, A., Soga, K., and Santamarina, C. (2012). "Factors affecting efficiency of microbially induced calcite precipitation." *J. Geotech. Geoenviron. Eng.*, 138(8), 992–1001.

Al-Thawadi, S. (2012). "Calcium carbonate crystals formation by ureolytic bacteria isolated from Australian soil and sludge." *J. Adv Sci. Eng. Res.*, 2(1), 12–26.

Arulanandan, K. and Perry, E. B. (1983). "Erosion in relation to filter design criteria in earth dams." *J. Geotech. Eng.*, 109(5), 682-298.

Bendahmane, F., Marot, D., and Alexis, A. (2008). "Experimental parametric study of suffusion and backward erosion." *J. Geotech. Geoenviron. Eng.*, 134(1), 57–67.

Chang, D., and Zhang, L. (2013a). "Critical hydraulic gradients of internal erosion under complex stress states." *J. Geotech. Geoenviron. Eng.*, 139(9), 1454–1467.

Chang, D., and Zhang, L. (2013b). "Extended internal stability criteria for soils under seepage." *Soils Found.*, 53(4), 569–583.

Chen, F., Deng, C., Song, W., Zhang, D., Al-Misned, F. A., Mortuza, M. G., Gadd, G. M., and Pan, X. (2016). "Biostabilization of desert sands using bacterially induced calcite precipitation." *Geomicrobiol. J.*, 33(3-4), 243-249.

Cheng, L., Cord-Ruwisch, R., and Shahin, M. A. (2013). "Cementation of sand soil by microbially induced calcite precipitation at various degrees of saturation." *Can. Geotech. J.*, 50(1), 81–90.

Cheng, L., Shanin, M., and Cord-Ruwisch, R. (2014). "Bio-cementation of sandy soil using microbially induced carbonate precipitation for marine environments." *Géotechnique*, 64(12), 1010–1013.

Cuthbert, M. O., McMillan, L. A, Handley-Sidhu, S., Riley, M. S., Tobler, D. J., and Phoenix, V. R. (2013). "A field and modeling study of fractured rock permeability reduction using microbially induced calcite precipitation." *Environ. Sci. Technol.*, 47(23), 13637–13643.

Daniel, D. E., Anderson, D. C., and Boynton, S. S. (1985). "Fixed-wall versus flexible-wall permeameters." *Hydraulic Barriers in Soil and Rock*, ASTM STP 874, Johnson et al. (Eds.), American Society for Testing and Materials, Philadelphia, pp. 107-126.

Danka, J. and Zhang, L. M. (2015). "Dike failure mechanisms and breaching parameters." *J. Geotech. Geoenviron. Eng.*, 141(9), 04015039.

Dawoud, O., Chen, C. Y., and Soga, K. (2014a). "Microbial induced calcite precipitation for geotechnical and environmental applications." *Proceedings of 2014 GeoShanghai International Congress: New Frontiers in Geotechnical Engineering*, G. Zhang and Z. Liu, eds., American Society of Civil Engineers, Shanghai, 11–18.

Dawoud, O., Chen, C. Y., and Soga, K. (2014b). "Microbial-induced calcite precipitation (MICP) using surfactants." *Proceedings of Geo-Congress 2014 Technical Papers: Geo-*

*Characterization and Modeling for Sustainability*, M. Abu-Farsakh and L. R. Hoyos, eds., American Society of Civil Engineers, Atlanta, 1635–1643.

DeJong, J. T., Mortensen, B. M., Martinez, B. C., and Nelson, D. C. (2010). “Bio-mediated soil improvement.” *Ecol. Eng.*, 36(2), 197–210.

DeJong, J. T., Martinez, B. C., Ginn, T. R., Hunt, C., Major, D., and Tanyu, B. (2014). “Development of scaled repeated five-spot treatment model for examining microbial induced calcite precipitation feasibility in field applications.” *Geotech. Test. J.*, 37(3), 1–12.

DeJong, J. T., and Montoya, B. M. (2013). “Healing of biologically induced cemented sands.” *Géotech. Lett.*, 3,147–151.

DeJong, J. T., Soga, K., Kavazanjian, E., et al. (2013). “Biogeochemical processes and geotechnical applications: progress, opportunities and challenges.” *Géotechnique*, 63(4), 287–301.

Engemoen, W. (2012). “Methods to mitigate internal erosion risks in existing embankment dams.” *Proceedings of 6th International Conference on Scour and Erosion*, Societe Hydrotechnique de France, Paris, 1567–1575.

Fannin, R. J., and Slangen, P. (2014). “On the distinct phenomena of suffusion and suffosion.” *Géotech. Lett.*, 4, 289–294.

Fell, R., MacGregor, P., Stapledon, D., and Bell, G. (2005). *Geotechnical Engineering of Dams*. Taylor & Francis Group plc, London, UK.

Feng, K. and Montoya, B. (2016). "Influence of confinement and cementation level on the behavior of microbial-induced calcite precipitated sands under monotonic drained loading." *J. Geotech. Geoenviron. Eng.*, 142(1), 04015057.

Ferris, F., Phoenix, V., Fujita, Y., and Smith, R. (2004). “Kinetics of calcite precipitation induced by ureolytic bacteria at 10 to 20 C in artificial groundwater.” *Geochim. Cosmochim. Ac.*, 67(8), 1701–1710.

Flora, A., Modoni, G., Lirer, S., and Croce, P. (2013). “The diameter of single, double and triple fluid jet grouting columns: prediction method and field trial results.” *Géotechnique*, 63(11), 934-945.

Flores-Berrones, R., Ramírez-Reynaga, M., and Macari, E. (2011). “Internal erosion and rehabilitation of an earth-rock dam.” *J. Geotech. Geoenviron. Eng.*, 137(2), 150-160.

Fonseva, J., Sim, W., Shire, T., and O’Sullivan, C. (2014). “Microstructural analysis of sands with varying degrees of internal stability.” *Géotechnique*, 64(5), 405–411.

Foster, M., and Fell, R. (2001). “Assessing embankment dam filters that do not satisfy design criteria.” *J. Geotech. Geoenviron. Eng.*, 127(5), 398–407.

Foster, M., Fell, R., and Spannagle, M. (2000). “The statistics of embankment dam failures and accidents.” *Can. Geotech. J.*, 37(5), 1000–1024.

Gomez, M. G., Martinez, B. C., DeJong, J. T., Hunt, C. E., deVlaming, L. A., Major, D. W., and Dworatzek, S. M. (2015). “Field-scale bio-cementation tests to improve sands.” *P. I. Civil. Eng.- Ground Improv.*, 168(3), 206-216.

Gruesbeck, C., and Collins, R. E. (1982). “Entrainment and deposition of fine particles in porous media.” *Soc. Petrol. Eng. J.*, 22(6), 847 – 856.

Haghighi, I., Chevalier, C., Duc, M., Guédon, S., and Reiffsteck, P. (2013). “Improvement of hole erosion test and results on reference soils.” *J. Geotech. Geoenviron. Eng.*, 139(2), 330–339.

Hata, T., Yokoyama, T., and Abe, H. (2013). “Investigation of a soil improvement technique for coastal regions on the basis of calcium carbonate precipitation by using the urea hydrolysis rate.” *Jpn. Geotech. J.*, 8(4), 505–515. (in Japanese)

Indraratna, B., Muttuvel, T., Khabbaz, H., and Armstrong, R. (2008). “Predicting the erosion rate of chemically treated soil using a process simulation apparatus for internal crack erosion.” *J. Geotech. Geoenviron. Eng.*, 134(6), 837–844.

Jiang, N. J., and Soga, K. (2014). “Seepage-induced erosion control by microbially induced calcite precipitation: An experimental investigation.” *Proceedings of 7th International Congress on Environmental Geotechnics*, A. Bouazza, S. T. S. Yuen, and B. Brown, eds., Engineers Australia, Melbourne, 1113–1120.

Jiang, N. J., Soga, K., and Dawoud, O. (2014). “Experimental study of mitigation of soil internal erosion by microbially induced calcite precipitation.” *GeoCongress 2014: Geo-Characterization and Modelling for Sustainability*, M. Abu-Farsakh, X. Yu, and L. R. Hoyos, eds., American Society of Civil Engineers, Atlanta, 1586–1595.

Jiang, N. J., Yoshioka, H., Yamamoto, K., and Soga, K. (2016). “Ureolytic activities of a urease-producing bacterium and purified urease enzyme in the anoxic condition: Implication for subseafloor sand production control by microbially induced carbonate precipitation (MICP).” *Ecol. Eng.*, 90, 96-104.

Ke, L., and Takahashi, A. (2012). “Strength reduction of cohesionless soil due to internal erosion induced by one-dimensional upward seepage flow.” *Soils Found.*, 52(4), 698–711.

Ke, L., and Takahashi, A. (2014). “Triaxial erosion test for evaluation of mechanical consequences of internal erosion.” *Geotech. Test. J.*, 37(2), 347–364.

Kenney, T. C., and Lau, D. (1985). “Internal stability of granular filters.” *Can. Geotech. J.*, 22(2), 215–225.

Khilar, K., Fogler, H., and Gray, D. (1985). “Model for piping-plugging in earthen structures.” *J. Geotech. Eng.*, 111(7), 833–846.

Krajewska, B. (2009). “Ureases I. Functional, catalytic and kinetic properties: A review.” *J. Mol. Catal. B-Enzym.*, 59(1-3), 9–21.

Lafleur, J., Mlynarek, J., and Rollin, A. (1989). “Filtration of broadly graded cohesionless soils.” *J. Geotech. Eng.*, 115(12), 1747–1768.

Lin, H., Suleiman, M., Brown, D., and Kavazanjian, E., Jr. (2016). "Mechanical behavior of sands treated by microbially induced carbonate precipitation." *J. Geotech. Geoenviron. Eng.*, 142(2), 04015066.

Marot, D., Bendahmane, F., Rosquoet, F., and Alexis, A. (2009). “Internal flow effects on isotropic confined sand-clay mixtures.” *Soil Sediment Contam.*, 18(3), 294–306.

Marot, D., Le, V. D., Garnier, J., Thorel, L., and Audrain, P. (2012). “Study of scale effect in an internal erosion mechanism: centrifuge model and energy analysis.” *Eur. J. Environ. Civil Eng.*, 16(1), 1–19.

Martin, D., Dodds, K., Ngwenya, B. T., Butler, I. B., and Elphick, S. C. (2012). “Inhibition of Sporosarcina pasteurii under anoxic conditions: implications for subsurface carbonate precipitation and remediation via ureolysis.” *Environ. Sci. Technol.*, 46(15), 8351–5.

Martinez, B., DeJong, J., Ginn, T., Montoya, B., Barkouki, T., Hunt, C., Tanyu, B., and Major, D. (2013). “Experimental optimization of microbial-induced carbonate precipitation for soil improvement.” *J. Geotech. Geoenviron. Eng.*, 139(4), 587–598.

Moffat, R., Fannin, R. J., and Garner, S. J. (2011). “Spatial and temporal progression of internal erosion in cohesionless soil.” *Can. Geotech. J.*, 48(3), 399–412.

Montoya, B., and DeJong, J. (2015). “Stress-strain behavior of sands cemented by microbially induced calcite precipitation.” *J. Geotech. Geoenviron. Eng.*,141(6), 04015019.

Montoya, B., DeJong, J., and Boulanger, R. (2013). “Dynamic response of liquefiable sand improved by microbial-induced calcite precipitation.” *Géotechnique*, 63(4), 302–312.

Phillips, A. J., Cunningham, A. B., Gerlach, R., Hiebert, R., Hwang, C., Lomans, B. P., Westrich, J., Mantilla, C., Kirksey, J., Esposito, R. A., and Spangler, L. (2016). “Fracture sealing with microbially-induced calcium carbonate precipitation: A field study.” *Environ. Sci. Technol.*, doi: 10.1021/acs.est.5b05559.

Rebata-Landa, V., and Santamarina, J. C. (2006). “Mechanical limits to microbial activity in deep sediments.” *Geochem. Geophy. Geosy.*, 7(11), Q11006.

Reddi, L., and Bonala, M. (1997). “Critical shear stress and its relationship with cohesion for sand. kaolinite mixtures.” *Can. Geotech. J.*, 34(1), 26–33.

Reddi, L., Lee, I., and Bonala, M. (2000). "Comparison of internal and surface erosion using flow pump tests on a sand-kaolinite mixture." *Geotech. Test. J.*, 23(1), 116–122.

Reddi, L., Ming, X., Hajra, M., and Lee, I. (2000). "Permeability reduction of soil filters due to physical clogging." *J. Geotech. Geoenviron. Eng.*, 126(3), 236–246.

Richards, K. S., and Reddy, K. R. (2007). "Critical appraisal of piping phenomena in earth dams." *B. Eng. Geol. Environ.*, 66(4), 381–402.

Seagren, E., and Aydilek, A. (2010). "Biomediated geomechanical processes." *Environmental Biology*, John Wiley and Sons, Inc., Hoboken, New Jersey, 319–349.

Shaikh, A., Ruff, J. F., Charlie, W. A., and Abt, S. R. (1988). "Erosion rate of dispersive and nondispersive clays." *J. Geotech. Eng.*, 114(5), 589-600.

Skempton, A. W., and Brogan, J. M. (1994). "Experiments on piping in sandy gravels." *Géotechnique*, 44(3), 449–460.

Soon, N. W., Lee, L. M., Khun, T. C., and Ling, H. S. (2014). "Factors affecting improvement in engineering properties of residual soil through microbial-induced calcite precipitation." *J. Geotech. Geoenviron. Eng.*, 140(5), 04014006.

Tomlinson, S. S., and Vaid, Y. P. (2000). "Seepage forces and confining pressure effects on piping erosion." *Can. Geotech. J.*, 37(1), 1–13.

USEPA. (2013). "Aquatic Life Ambient Water Quality Criteria for Ammonia - Freshwater." USA Environmental Protection Agency, Washington D.C.

USSD. (2011). "Materials for Embankment Dams." United States Society on Dams, Denver, CO.

van Paassen, L. A., Ghose, R., van der Linden, T. J. M., van der Star, W. R. L., and van Loosdrecht, M. C. M. (2010). "Quantifying biomediated ground improvement by ureolysis: large-scale biogrout experiment." *J. Geotech. Geoenviron. Eng.*, 136(12), 1721-1728.

Wan, C. F., and Fell, R. (2004). "Investigation of rate of erosion of soils in embankment dams." *J. Geotech. Geoenviron. Eng.* 130(4), 373–380.

Wan, C. F., and Fell, R. (2008). "Assessing the potential of internal instability and suffusion in embankment dams and their foundations." *J. Geotech. Geoenviron. Eng.* 134(3), 401–407.

Whiffin, V. S. (2004). "Microbial $CaCO_3$ precipitation for the production of biocement." Murdoch University, Perth, Australia.

Whiffin, V. S., van Paassen, L. A., and Harkes, M. P. (2007). "Microbial carbonate precipitation as a soil improvement technique." *Geomicrobiol. J.*, 24(5), 417–423.

Xiao, M., and Shwiyhat, N. (2012). "Experimental investigation of the effects of suffusion on physical and geomechanic characteristics of sandy soils." *Geotech. Test. J.*, 35(6), 890–900.

**Table 1** Stability characterization for sand-clay mixtures in this study

| Soil properties | | Sand-clay mixture | | |
|---|---|---|---|---|
| | | **BB** | **CB** | **DE** |
| Coarse fraction | Soil type | Sand B | Sand C | Sand D |
| | Content, w/w (%) | 80 | 80 | 80 |
| | $D_{min}$ (μm) [1] | 450 | 285 | 130 |
| Fine fraction | Soil type | Kaolin B | Kaolin B | Kaolin E |
| | Content, w/w (%) | 20 | 20 | 20 |
| | $d_{max}$ (μm) [2] | 21 | 21 | 21 |
| Internal stability analysis | Gap ratio, $G_r$ | 21.4 | 13.6 | 6.2 |
| | Stability criterion [3] | 6 | 6 | 6 |
| | Stability | U [4] | U | U |

[1] the minimum particle size of the coarse fraction in the particle size distribution curve;
[2] the maximum particle size of the fine fraction in the particle size distribution curve;
[3] $G_r<0.3P$, $P$ is the fine content (20% in this study);
[4] Internally unstable.

**List of Figure Captions**

**Fig. 1** Particle size distribution curves for sands, kaolin-clays, and their mixtures

**Fig. 2** Schematic diagram of the rigid-wall column erosion test apparatus ((a). seepage erosion test system; (b). the Plexiglas rigid-wall column)

**Fig. 3** Schematic illustration of MICP treatment procedure (PV: pore volume of tested soils; M1, M2 and M3: MICP treatment strategies 1, 2 and 3)

**Fig. 4** Schematic illustration of the internal erosion test progress

**Fig. 5** Visual observations of sand-clay mixture during the internal erosion test ((a)~(d): untreated soils; (e)~(h): MICP treated soils)

**Fig. 6** Variations of clay concentration in the effluent solution with flow volume ((a). CB_U; (b) CB_M1)

**Fig. 7** Correlations between peak erosion rate and shear stress ((a) BB; (b) CB; (c) DE)

**Fig. 8** Erosion coefficient ($\alpha$) based on Equation (6)

**Fig. 9** Coupling relationships between permeability, volumetric contraction and accumulative erosion weight during internal erosion process ((a) BB; (b) CB; (c) DE)

**Fig. 10** Coupling relationships between permeability and volumetric contraction during internal erosion process ((a) BB; (b) CB; (c) DE)

**Fig. 11** Evolutions of pH, EC and c[$NH_4^+$] in effluent solution with time (BB_M2 and BB_U)

**Fig. 12** MICP performance of internal erosion control in sand-clay mixtures with different gap ratios

**Fig. 13** Carbonate precipitation contents and MICP treatment efficiency for sand-clay mixtures with different gap ratios

**Fig. 14** Correlations between normalized erosion coefficient and carbonate precipitation content

**Fig. 15** Profiles of carbonate precipitation along the depth of the MICP treated soils

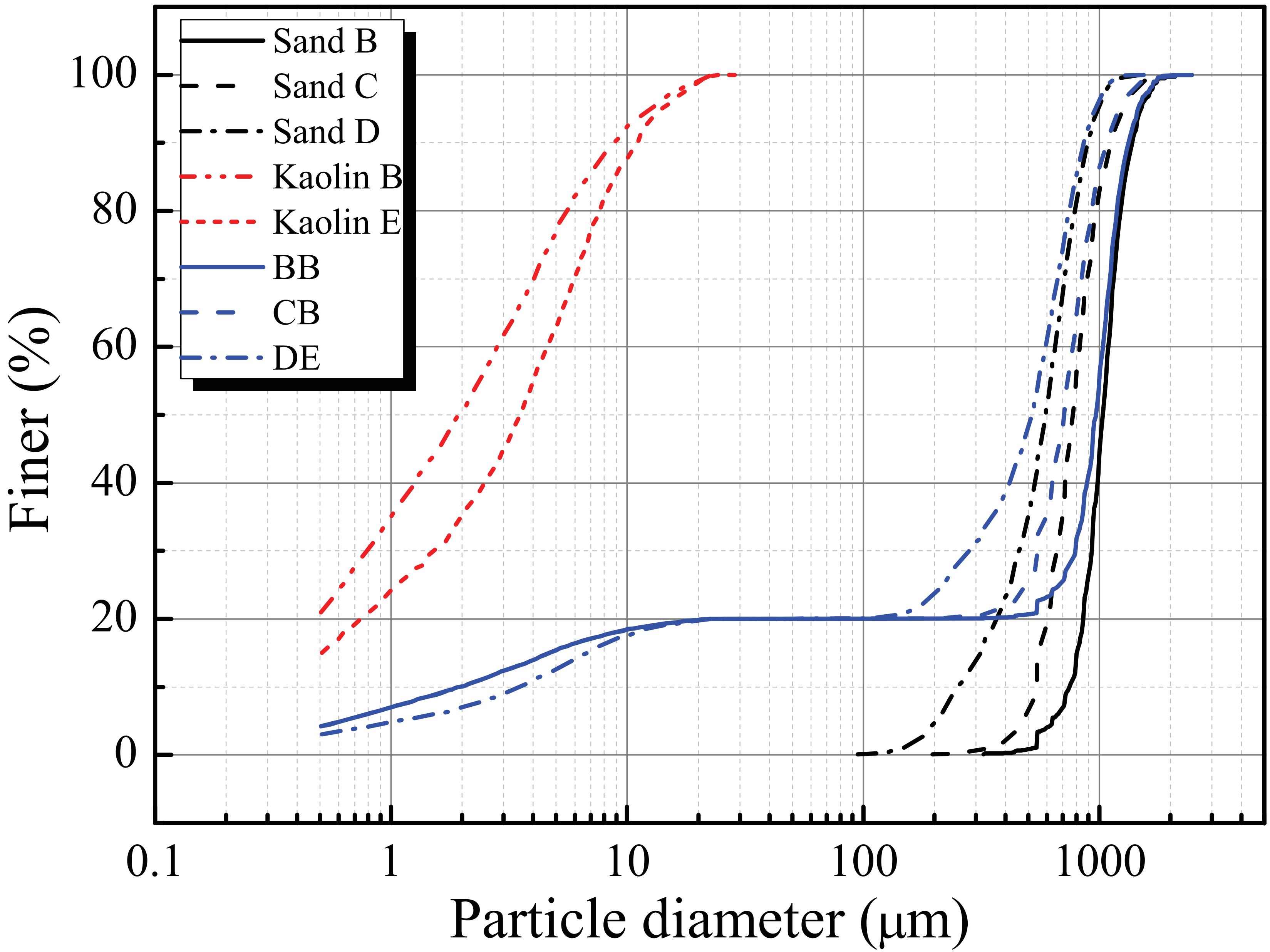
Sand B
Sand C
Sand D
Kaolin B
Kaolin E
BB
CB
DE
Finer (%)
100
80
60
40
20
0
0.1
1
10
100
1000
Particle diameter (μm)

Figure 2(a)



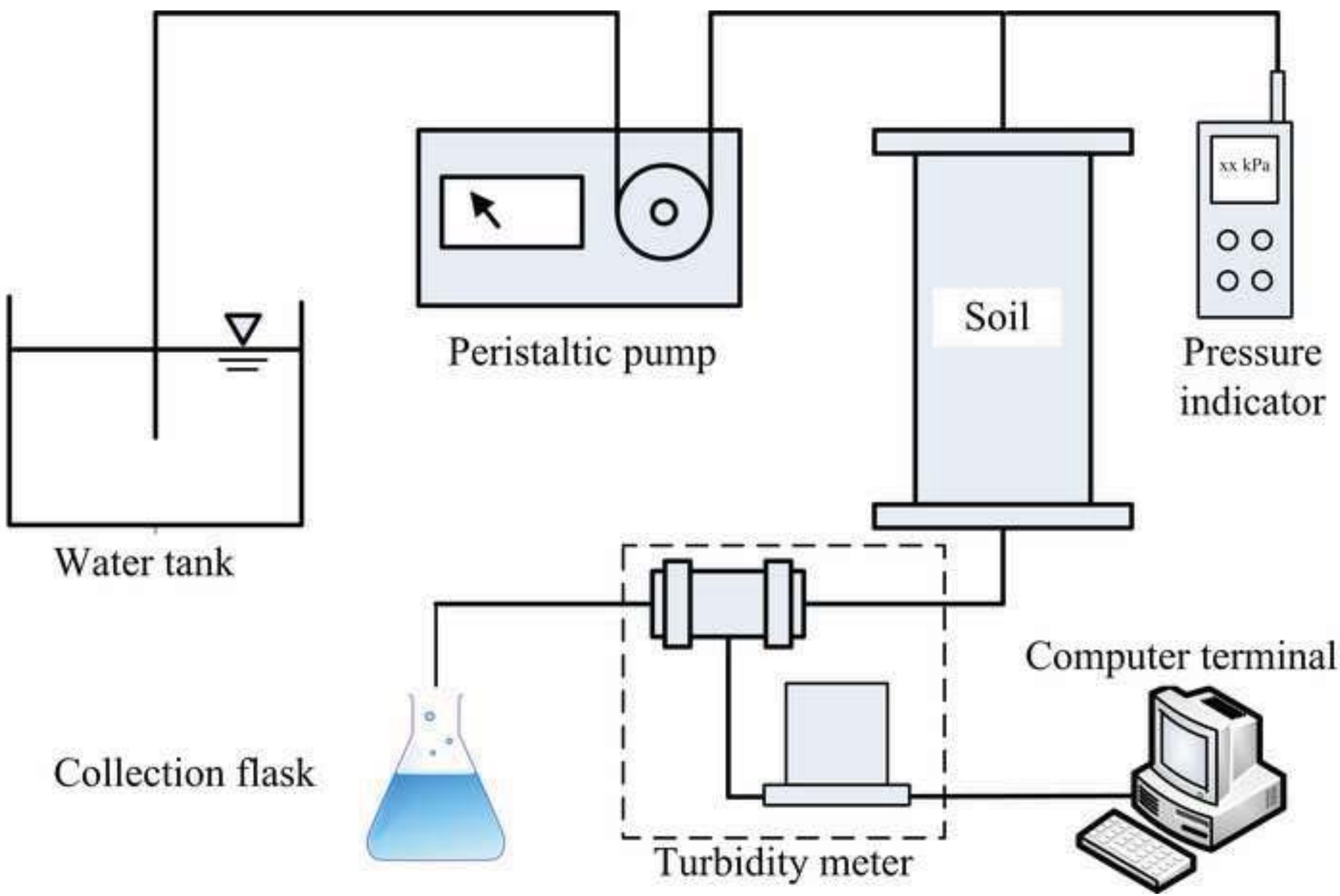
Peristaltic pump
Soil
xx kPa
Pressure
indicator
Water tank
Computer terminal
Collection flask
Turbidity meter

Figure 2(b)

Click here to download Figure Fig 2b.tif

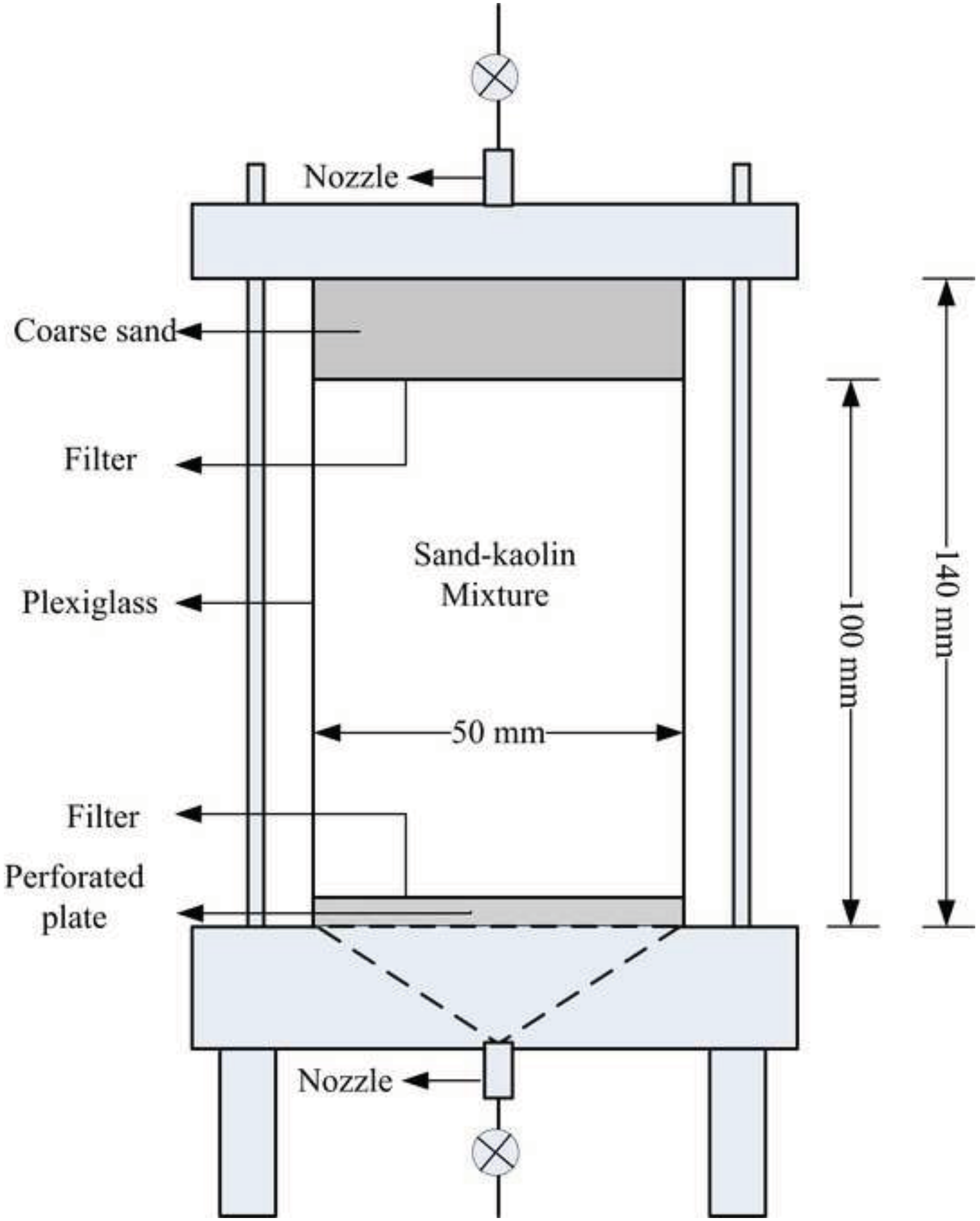

Figure 3



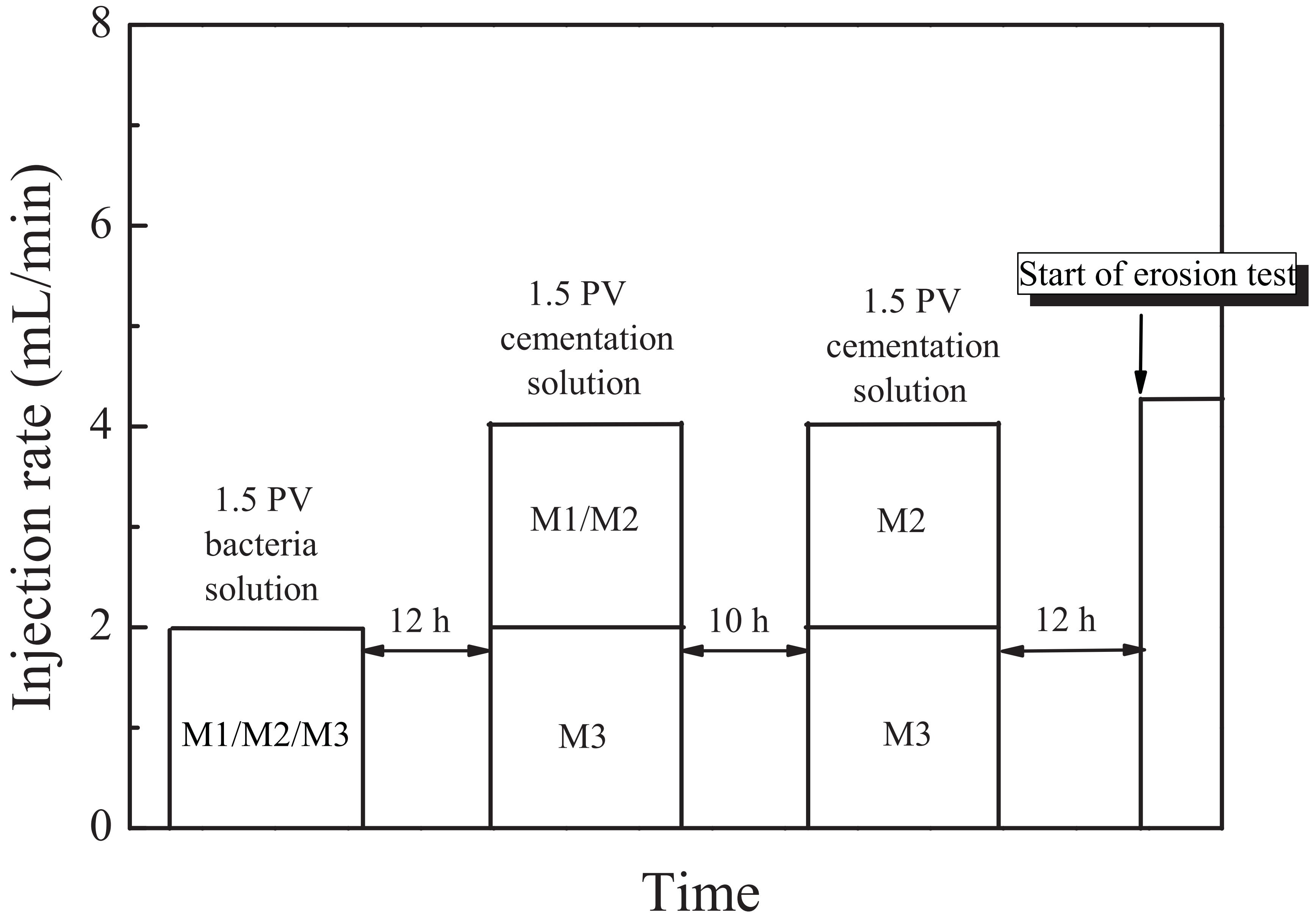
Injection rate (mL/min)
0
2
4
6
8
Time
1.5 PV
bacteria
solution
M1/M2/M3
12 h
1.5 PV
cementation
solution
M1/M2
M3
10 h
1.5 PV
cementation
solution
M2
M3
12 h
Start of erosion test

Figure 4



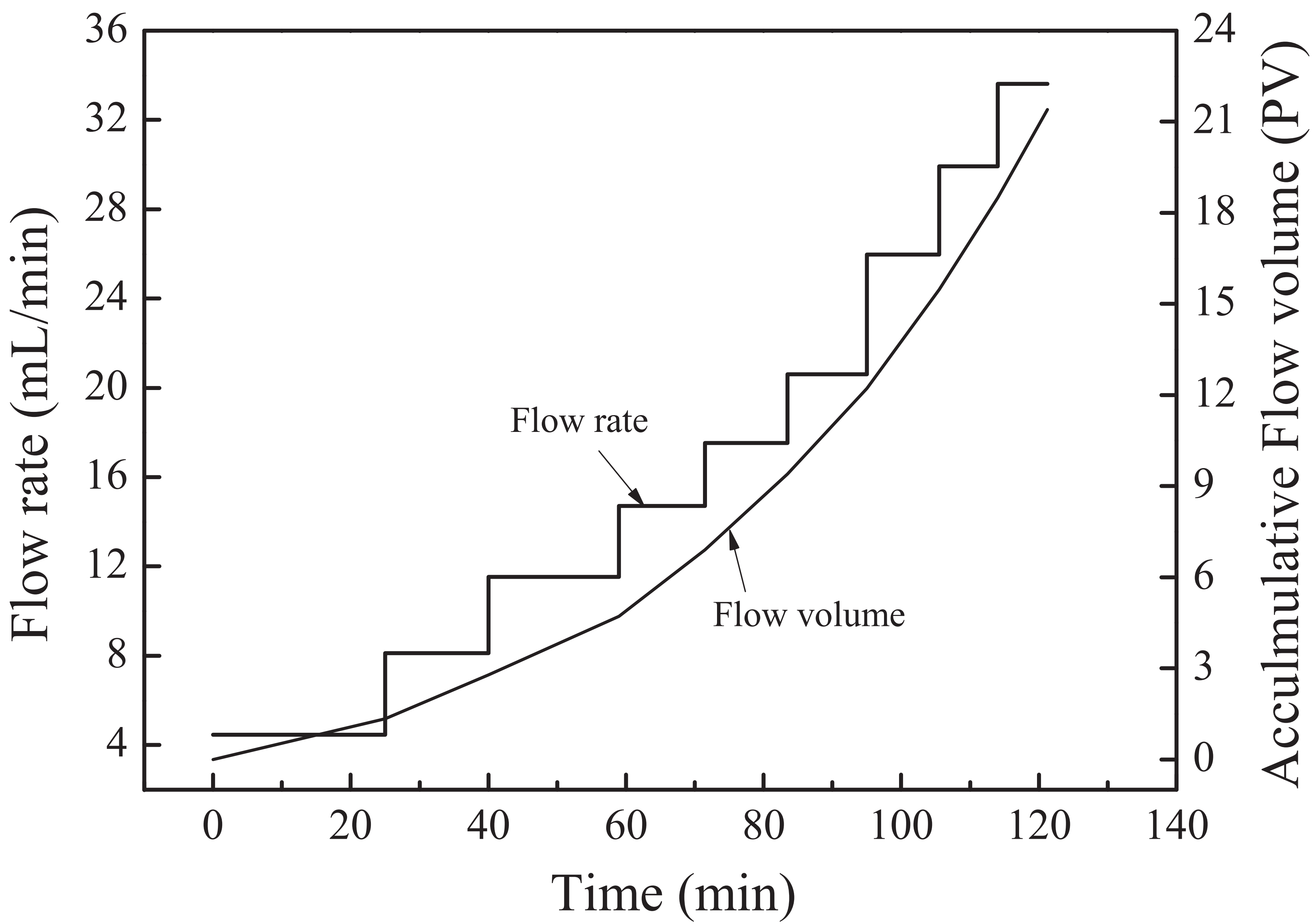
Flow rate (mL/min)
Accumulative Flow volume (PV)
Time (min)
Flow rate
Flow volume
36
32
28
24
20
16
12
8
4
24
21
18
15
12
9
6
3
0
0
20
40
60
80
100
120
140


(a) CB_U, 4.47 mL/min
(b) CB_U, 11.54 mL/min
(c) CB_U, 20.61 mL/min
(d) CB_U, 33.61 mL/min
(e) CB_M1, 4.47 mL/min
(f) CB_M1, 11.54 mL/min
(g) CB_M1, 20.61 mL/min
(h) CB_M1, 33.61 mL/min

Figure 6(a)

Click here to download Figure Fig 6a.eps

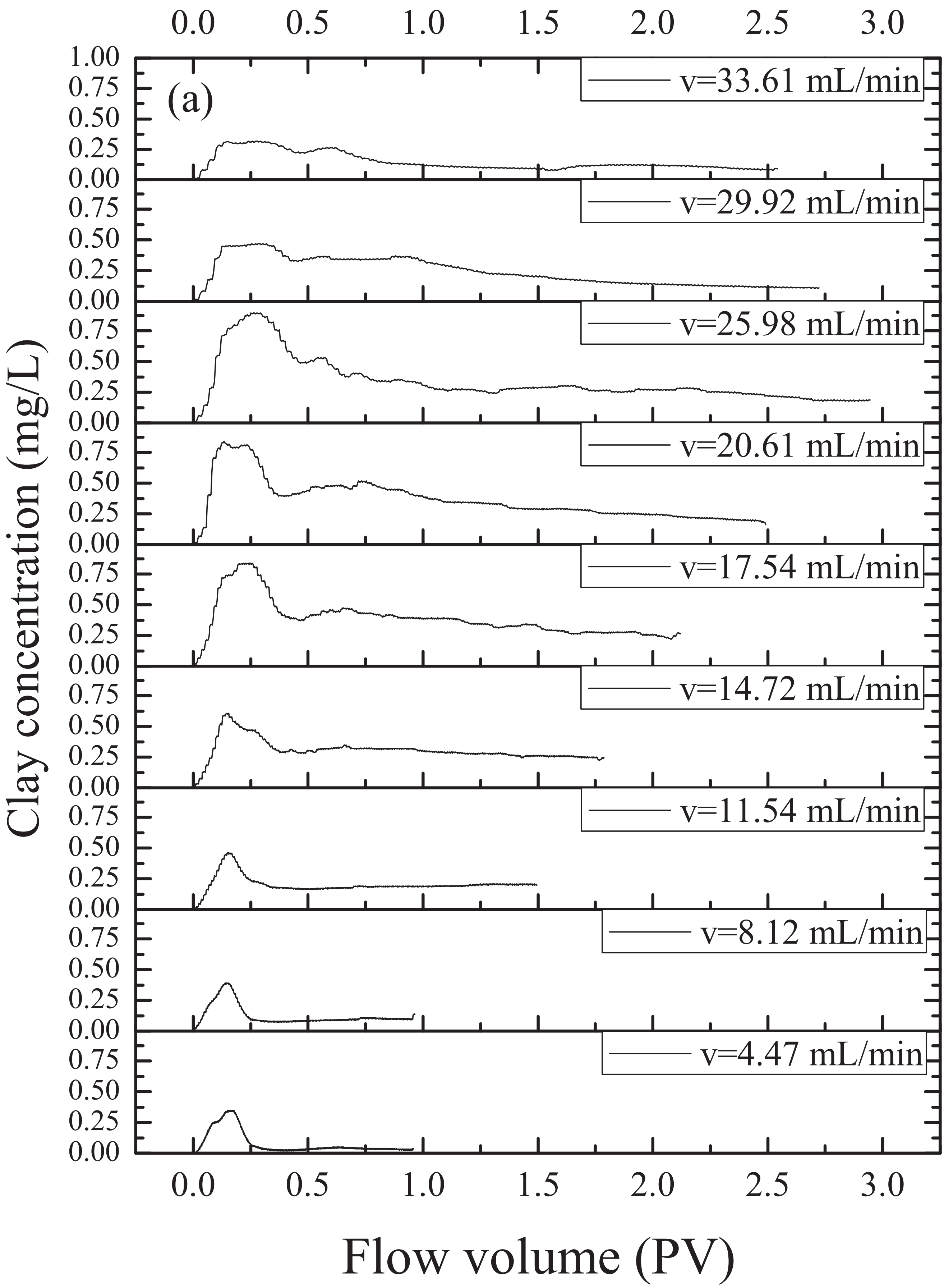

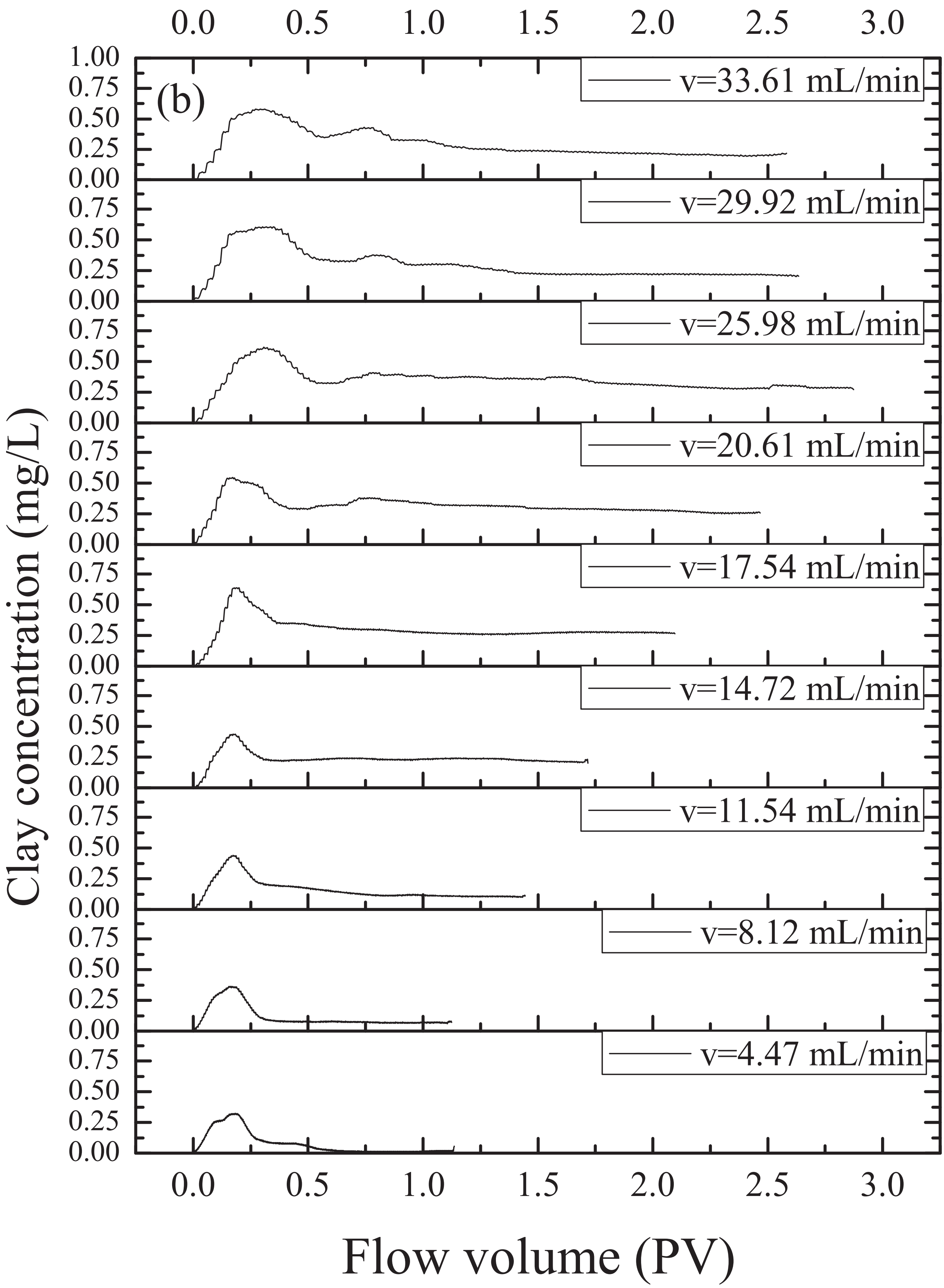
(b)
v=33.61 mL/min
v=29.92 mL/min
v=25.98 mL/min
v=20.61 mL/min
v=17.54 mL/min
v=14.72 mL/min
v=11.54 mL/min
v=8.12 mL/min
v=4.47 mL/min
Clay concentration (mg/L)
Flow volume (PV)
0.0
0.5
1.0
1.5
2.0
2.5
3.0
1.00
0.75
0.50
0.25
0.00

Figure 7(a)



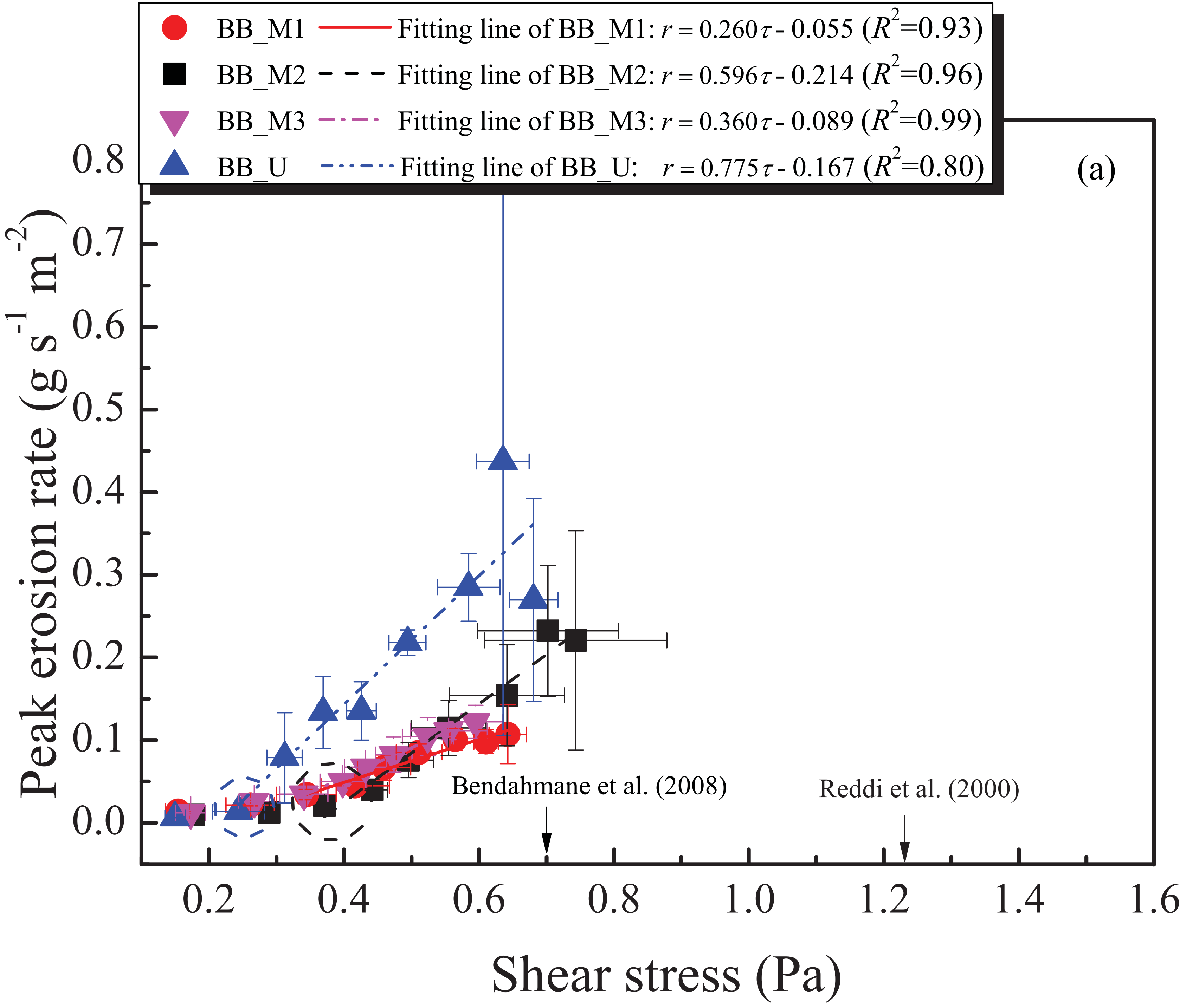
BB_M1
Fitting line of BB_M1: $r = 0.260\tau - 0.055$ ($R^2$=0.93)
BB_M2
Fitting line of BB_M2: $r = 0.596\tau - 0.214$ ($R^2$=0.96)
BB_M3
Fitting line of BB_M3: $r = 0.360\tau - 0.089$ ($R^2$=0.99)
BB_U
Fitting line of BB_U: $r = 0.775\tau - 0.167$ ($R^2$=0.80)
(a)
Peak erosion rate (g s$^{-1}$ m$^{-2}$)
0.0
0.1
0.2
0.3
0.4
0.5
0.6
0.7
0.8
Bendahmane et al. (2008)
Reddi et al. (2000)
0.2
0.4
0.6
0.8
1.0
1.2
1.4
1.6
Shear stress (Pa)

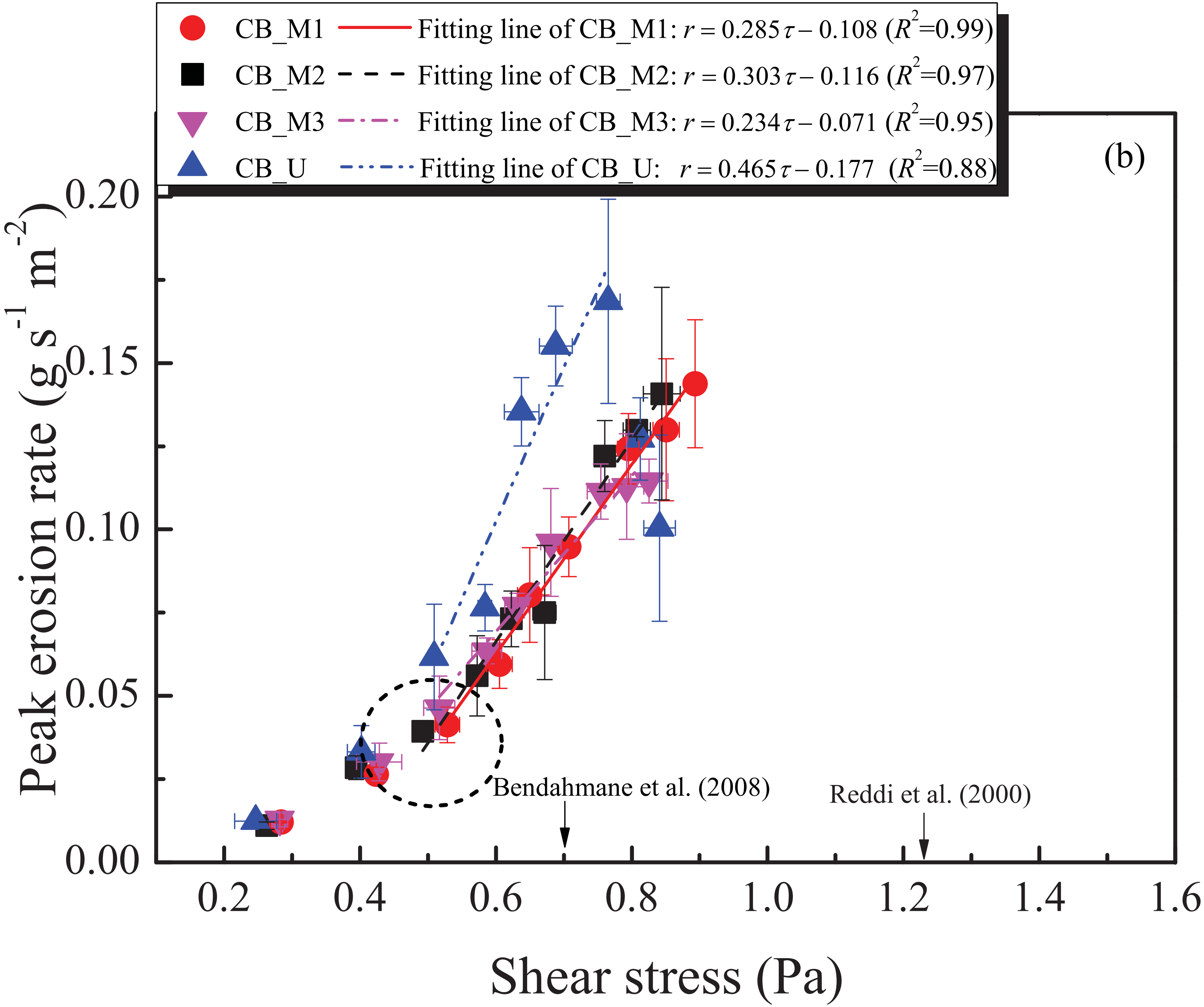
CB_M1
Fitting line of CB_M1: r = 0.285τ – 0.108 (R2=0.99)
CB_M2
Fitting line of CB_M2: r = 0.303τ – 0.116 (R2=0.97)
CB_M3
Fitting line of CB_M3: r = 0.234τ – 0.071 (R2=0.95)
CB_U
Fitting line of CB_U: r = 0.465τ – 0.177 (R2=0.88)
(b)
Peak erosion rate (g s-1 m-2)
0.20
0.15
0.10
0.05
0.00
Bendahmane et al. (2008)
Reddi et al. (2000)
0.2
0.4
0.6
0.8
1.0
1.2
1.4
1.6
Shear stress (Pa)

Figure 7(c)



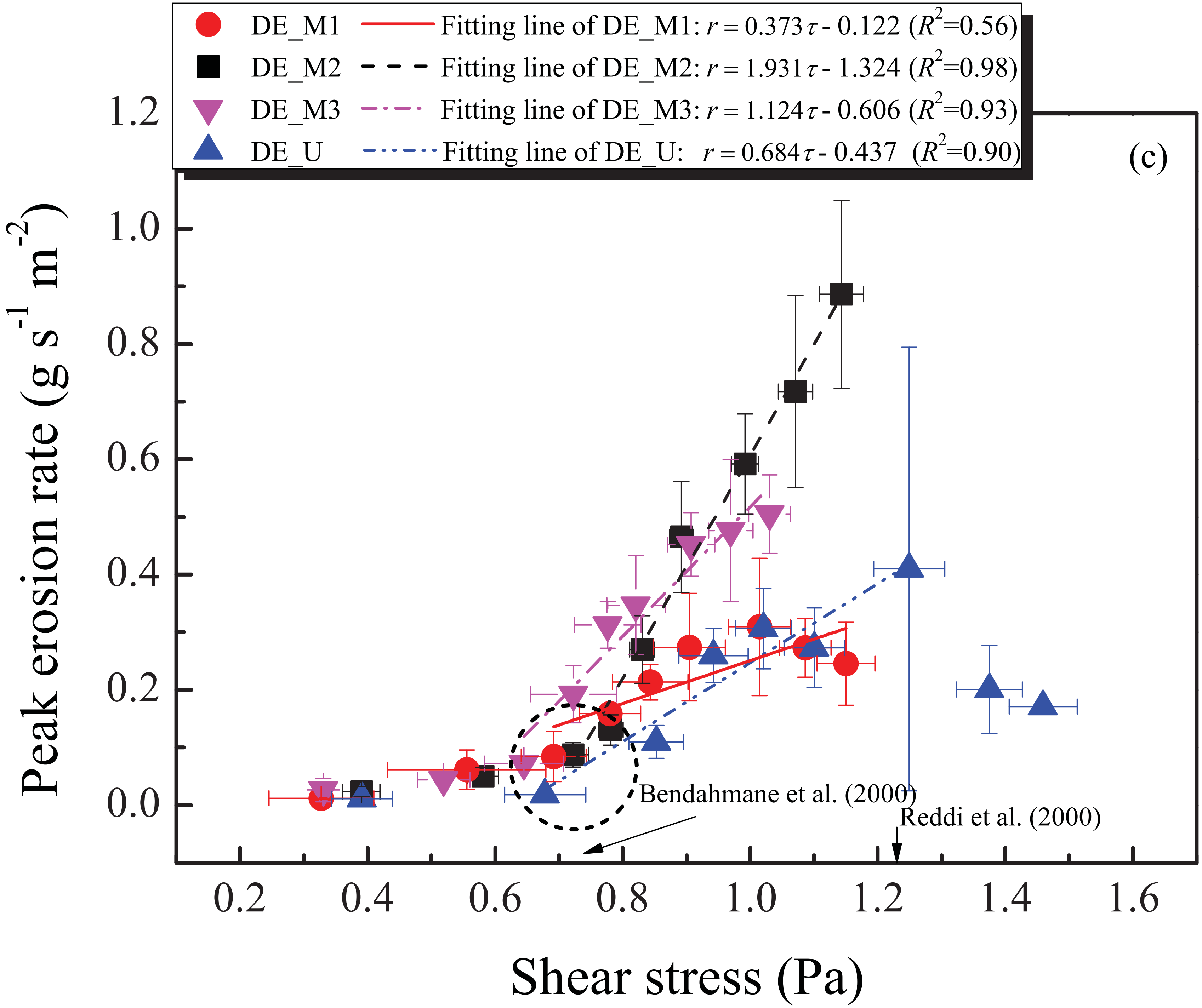
DE_M1
Fitting line of DE_M1: $r = 0.373\tau - 0.122$ ($R^2$=0.56)
DE_M2
Fitting line of DE_M2: $r = 1.931\tau - 1.324$ ($R^2$=0.98)
DE_M3
Fitting line of DE_M3: $r = 1.124\tau - 0.606$ ($R^2$=0.93)
DE_U
Fitting line of DE_U: $r = 0.684\tau - 0.437$ ($R^2$=0.90)
(c)
Bendahmane et al. (2000)
Reddi et al. (2000)
Peak erosion rate (g s$^{-1}$ m$^{-2}$)
Shear stress (Pa)
0.0
0.2
0.4
0.6
0.8
1.0
1.2
0.2
0.4
0.6
0.8
1.0
1.2
1.4
1.6

Figure 8



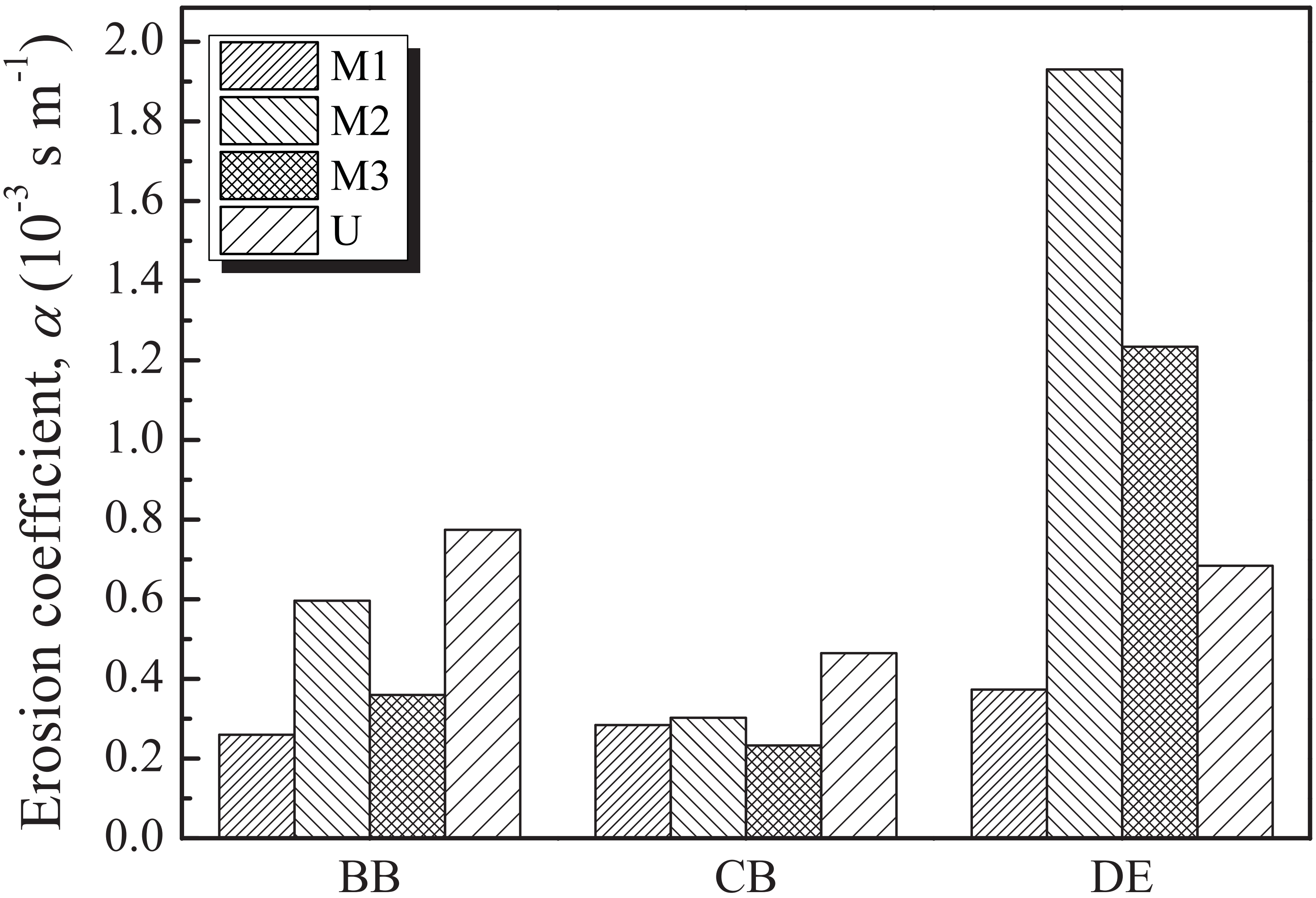
Erosion coefficient, α (10-3 s m-1)
2.0
1.8
1.6
1.4
1.2
1.0
0.8
0.6
0.4
0.2
0.0
M1
M2
M3
U
BB
CB
DE

Figure 9(a)



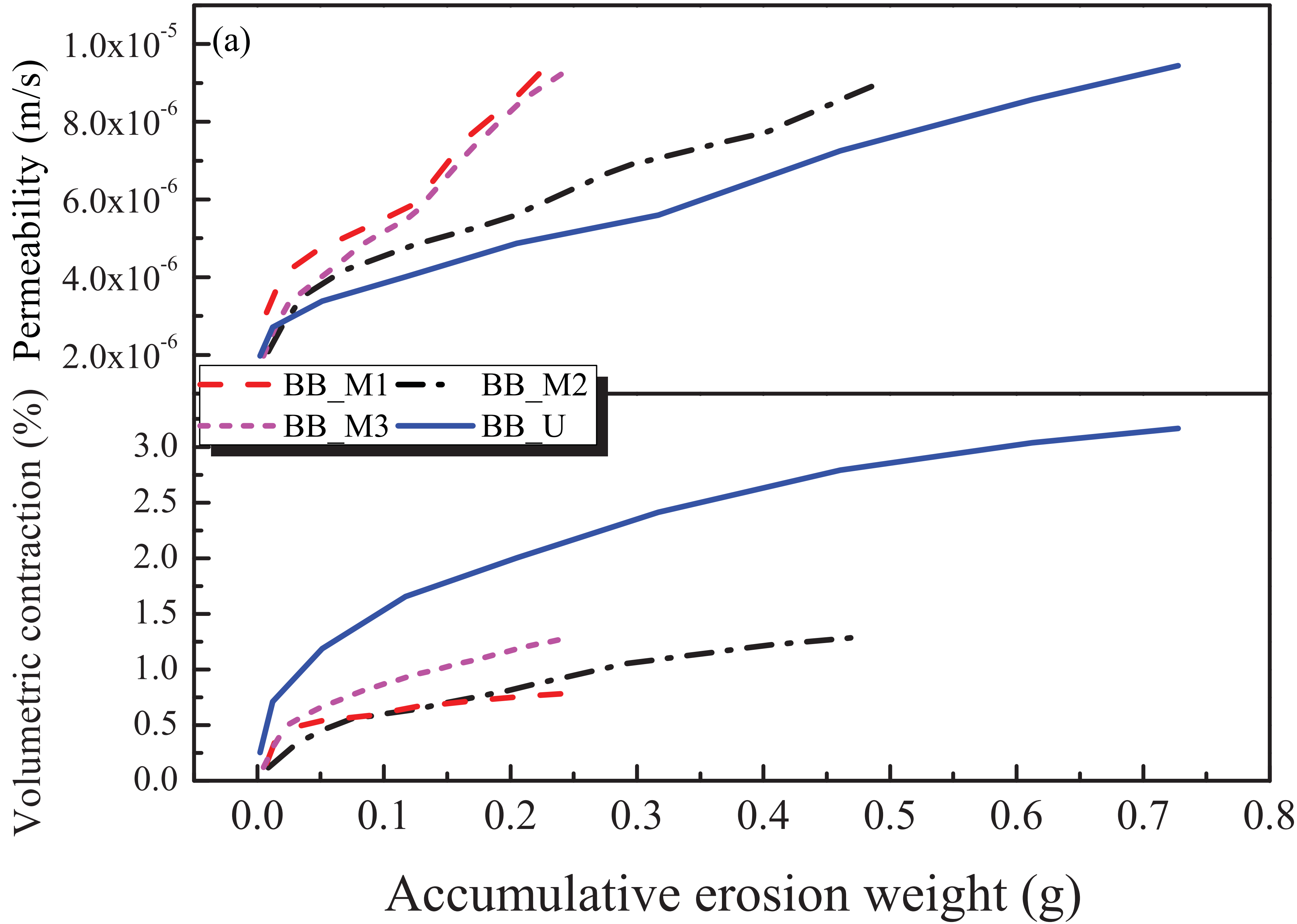
(a)
Permeability (m/s)
1.0x10^-5
8.0x10^-6
6.0x10^-6
4.0x10^-6
2.0x10^-6
BB_M1
BB_M2
BB_M3
BB_U
Volumetric contraction (%)
3.0
2.5
2.0
1.5
1.0
0.5
0.0
0.0
0.1
0.2
0.3
0.4
0.5
0.6
0.7
0.8
Accumulative erosion weight (g)

Figure 9(b)



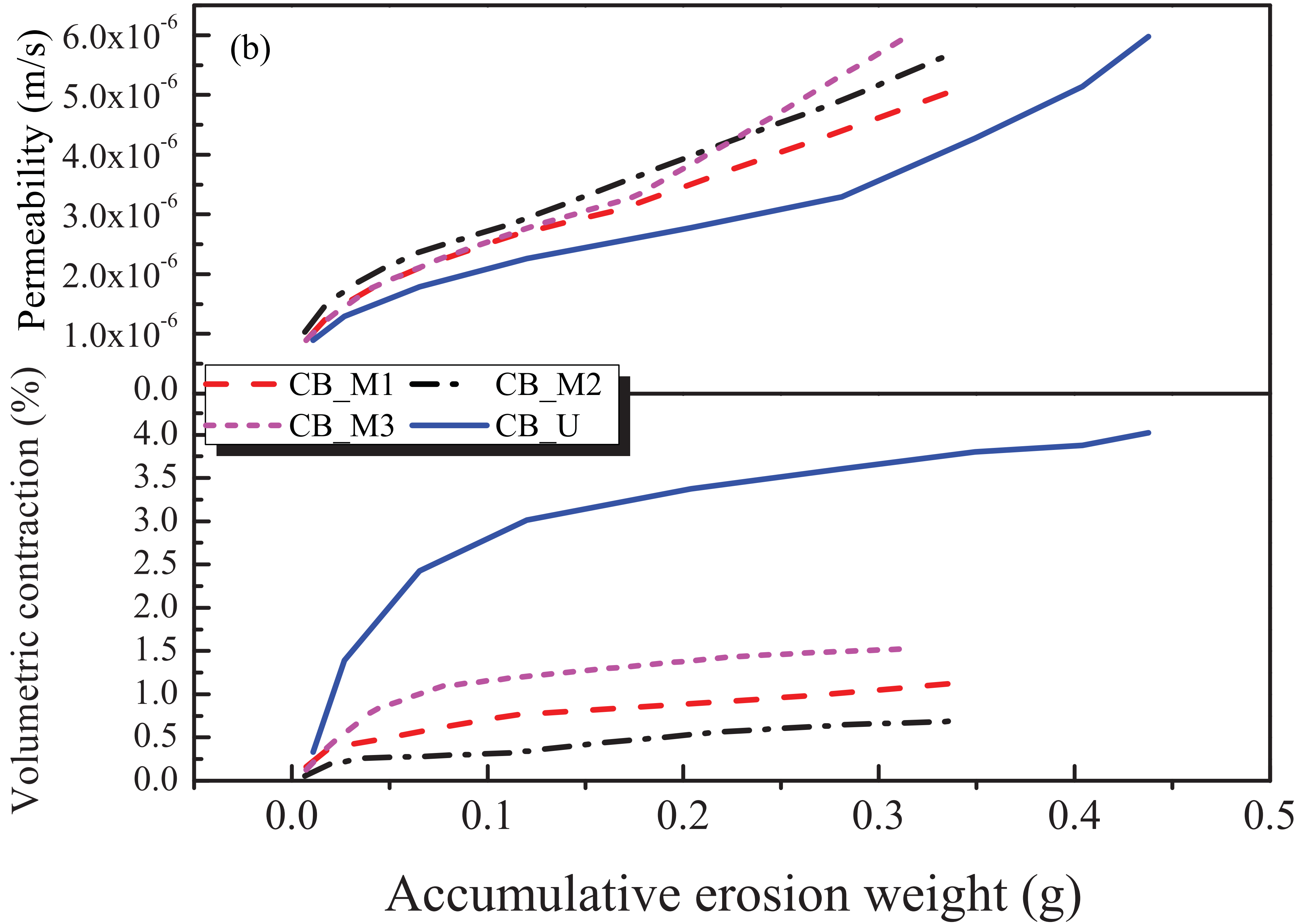

(b)
Permeability (m/s)
6.0x10^-6
5.0x10^-6
4.0x10^-6
3.0x10^-6
2.0x10^-6
1.0x10^-6
CB_M1
CB_M2
CB_M3
CB_U
Volumetric contraction (%)
0.0
0.5
1.0
1.5
2.0
2.5
3.0
3.5
4.0
0.1
0.2
0.3
0.4
0.5
Accumulative erosion weight (g)

Figure 9(c)



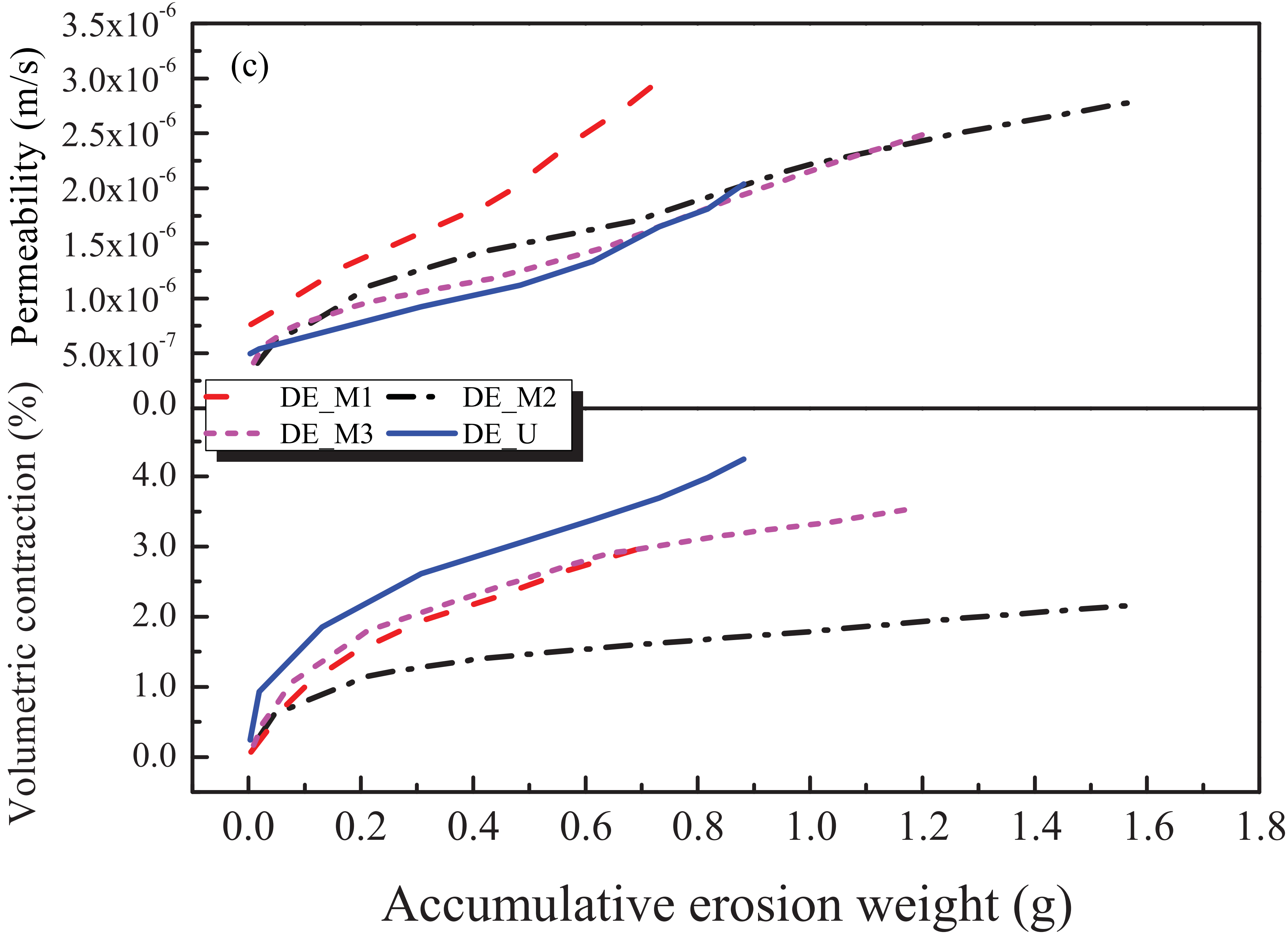
(c)
Permeability (m/s)
3.5x10^-6
3.0x10^-6
2.5x10^-6
2.0x10^-6
1.5x10^-6
1.0x10^-6
5.0x10^-7
0.0
Volumetric contraction (%)
4.0
3.0
2.0
1.0
0.0
DE_M1
DE_M2
DE_M3
DE_U
0.0
0.2
0.4
0.6
0.8
1.0
1.2
1.4
1.6
1.8
Accumulative erosion weight (g)

Figure 10

Click here to download Figure Fig 10.eps

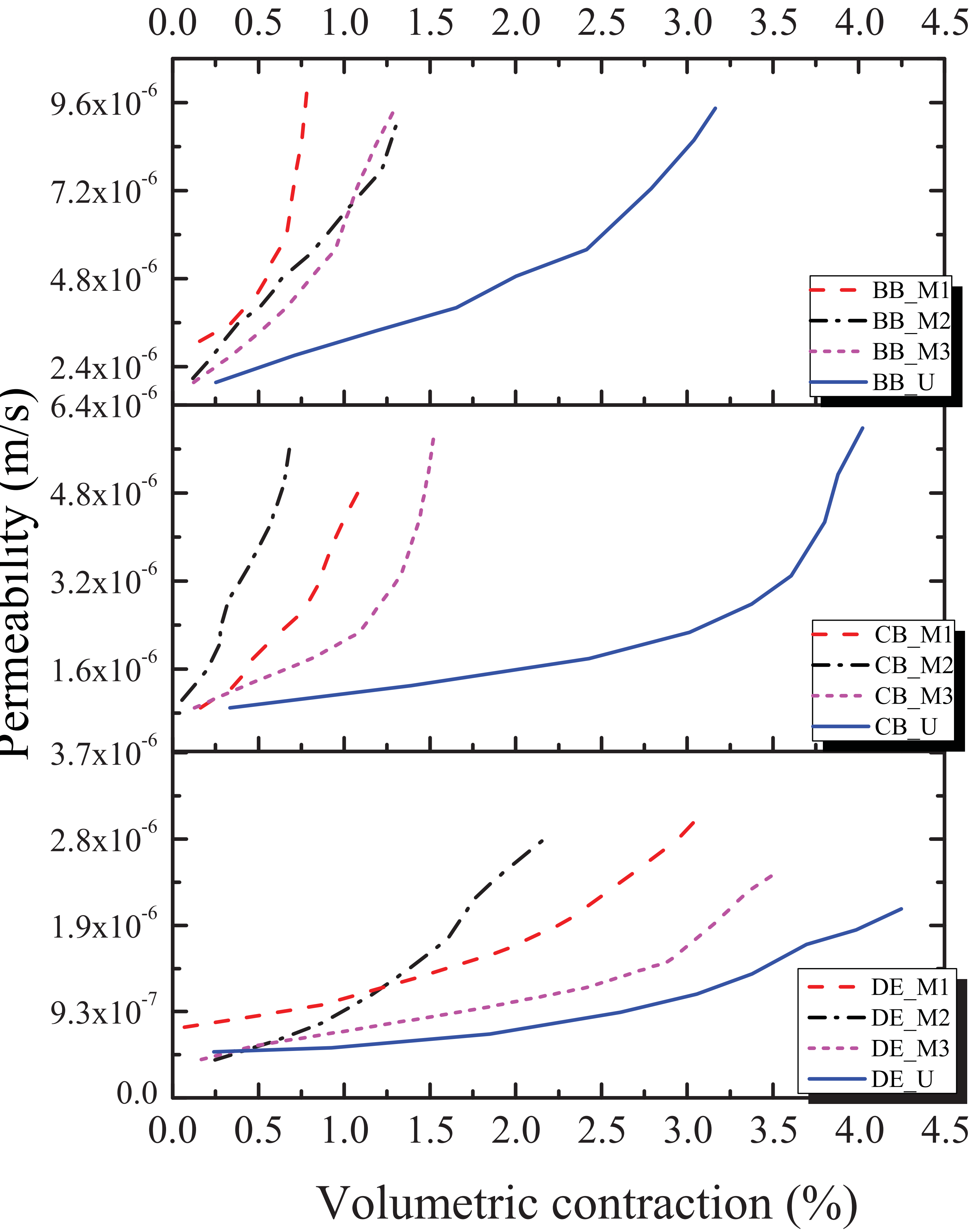

Figure 11



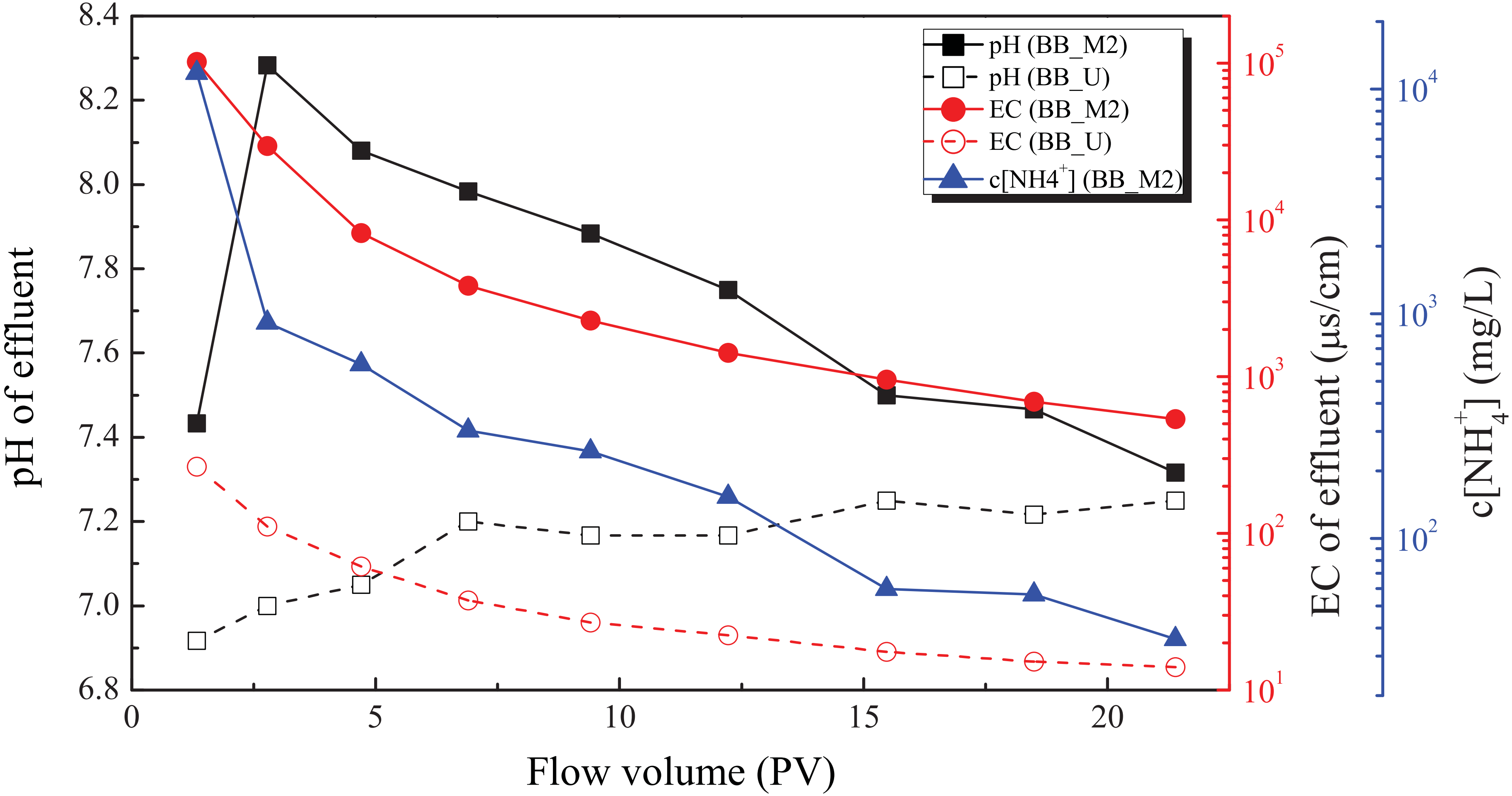
pH (BB_M2)
pH (BB_U)
EC (BB_M2)
EC (BB_U)
c[NH4$^+$] (BB_M2)
pH of effluent
8.4
8.2
8.0
7.8
7.6
7.4
7.2
7.0
6.8
0
5
10
15
20
Flow volume (PV)
EC of effluent (μs/cm)
$10^5$
$10^4$
$10^3$
$10^2$
$10^1$
$c[NH_4^+]$ (mg/L)
$10^4$
$10^3$
$10^2$

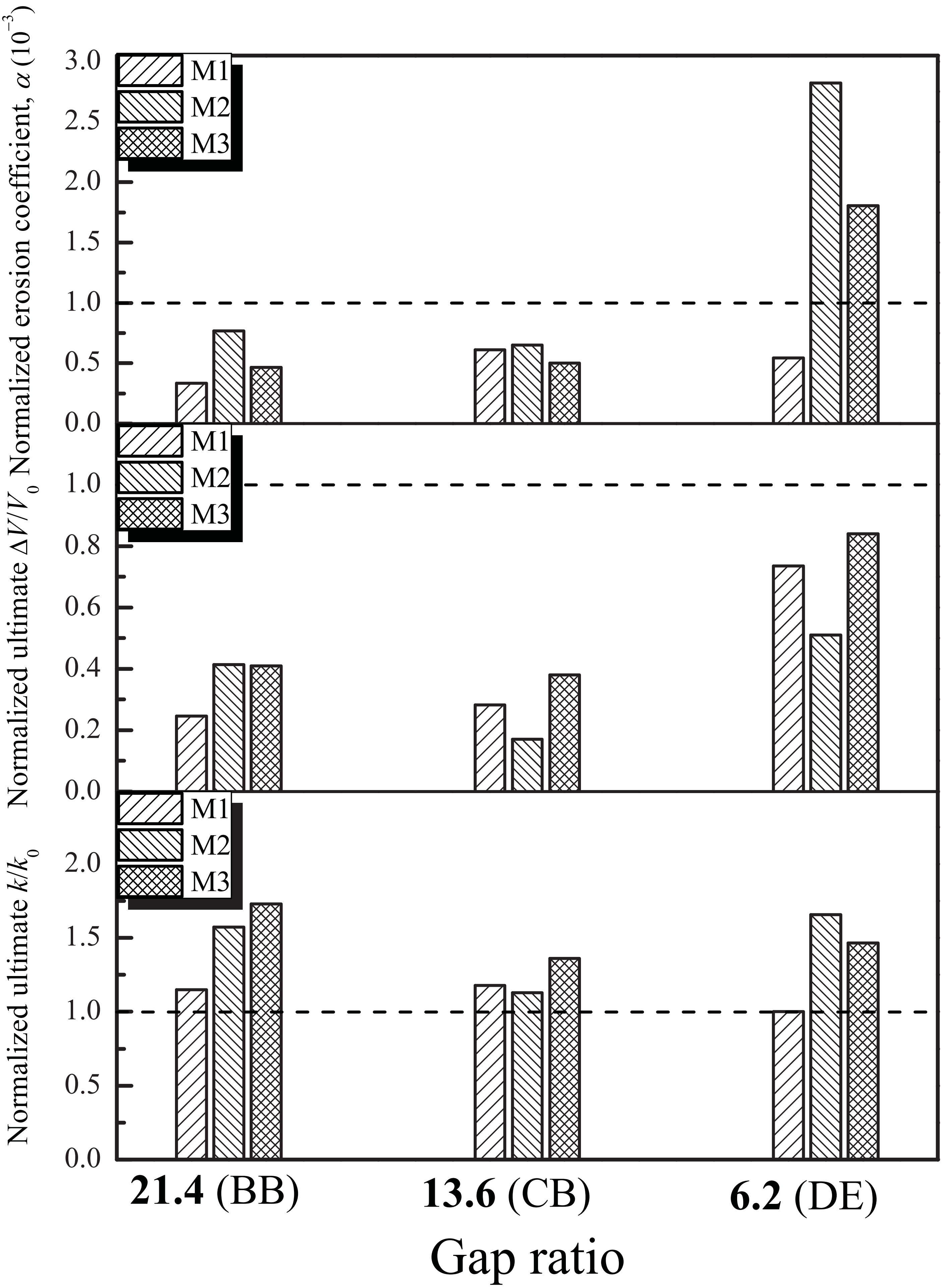

Normalized erosion coefficient, $\alpha$ ($10^{-3}$)
Normalized ultimate $\Delta V/V_0$
Normalized ultimate $k/k_0$
M1
M2
M3
3.0
2.5
2.0
1.5
1.0
0.5
0.0
0.8
0.6
0.4
0.2
**21.4** (BB)
**13.6** (CB)
**6.2** (DE)
Gap ratio

Figure 13



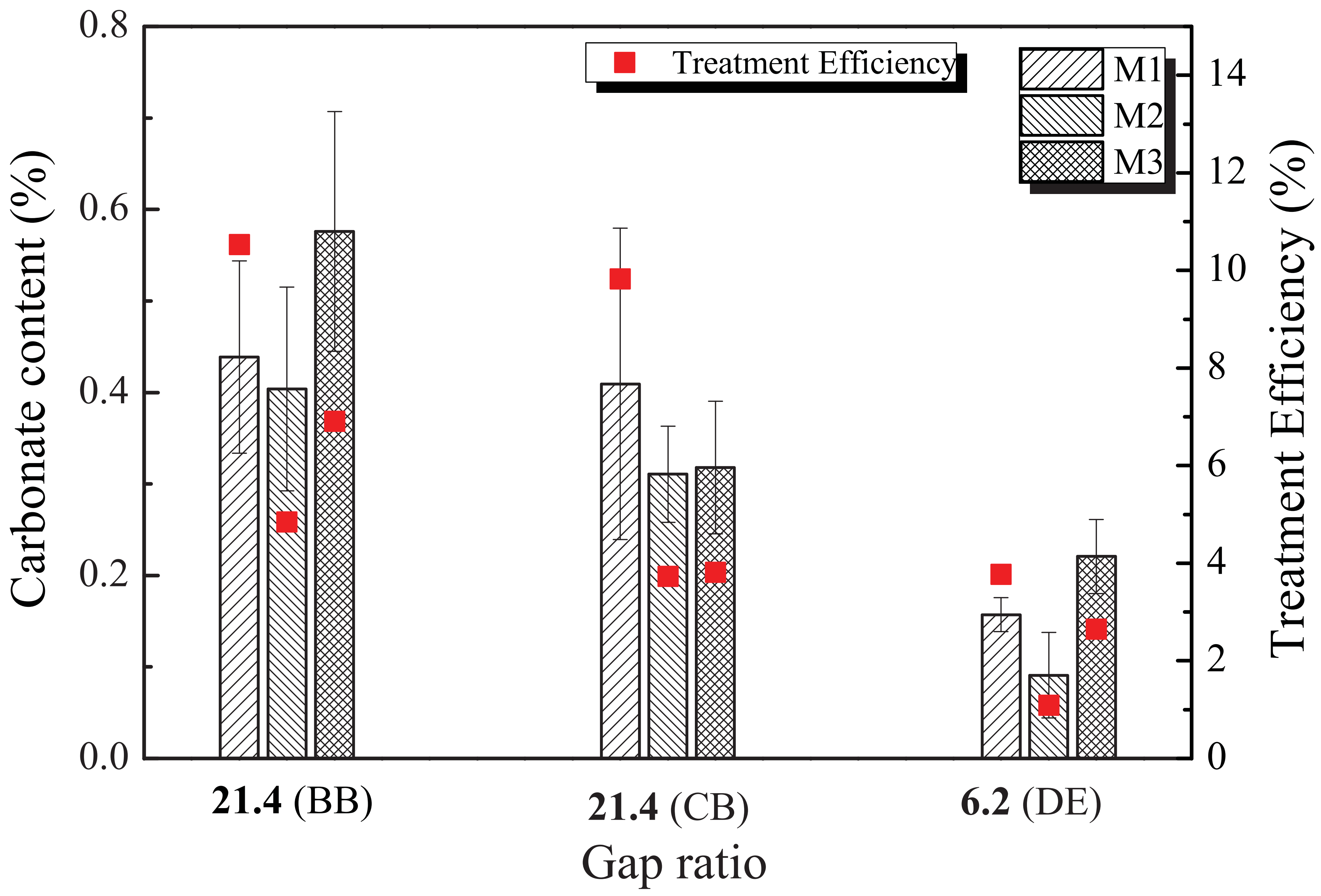

Carbonate content (%)
0.8
0.6
0.4
0.2
0.0
Treatment Efficiency
M1
M2
M3
14
12
10
8
6
4
2
0
Treatment Efficiency (%)
21.4 (BB)
21.4 (CB)
6.2 (DE)
Gap ratio

Figure 14



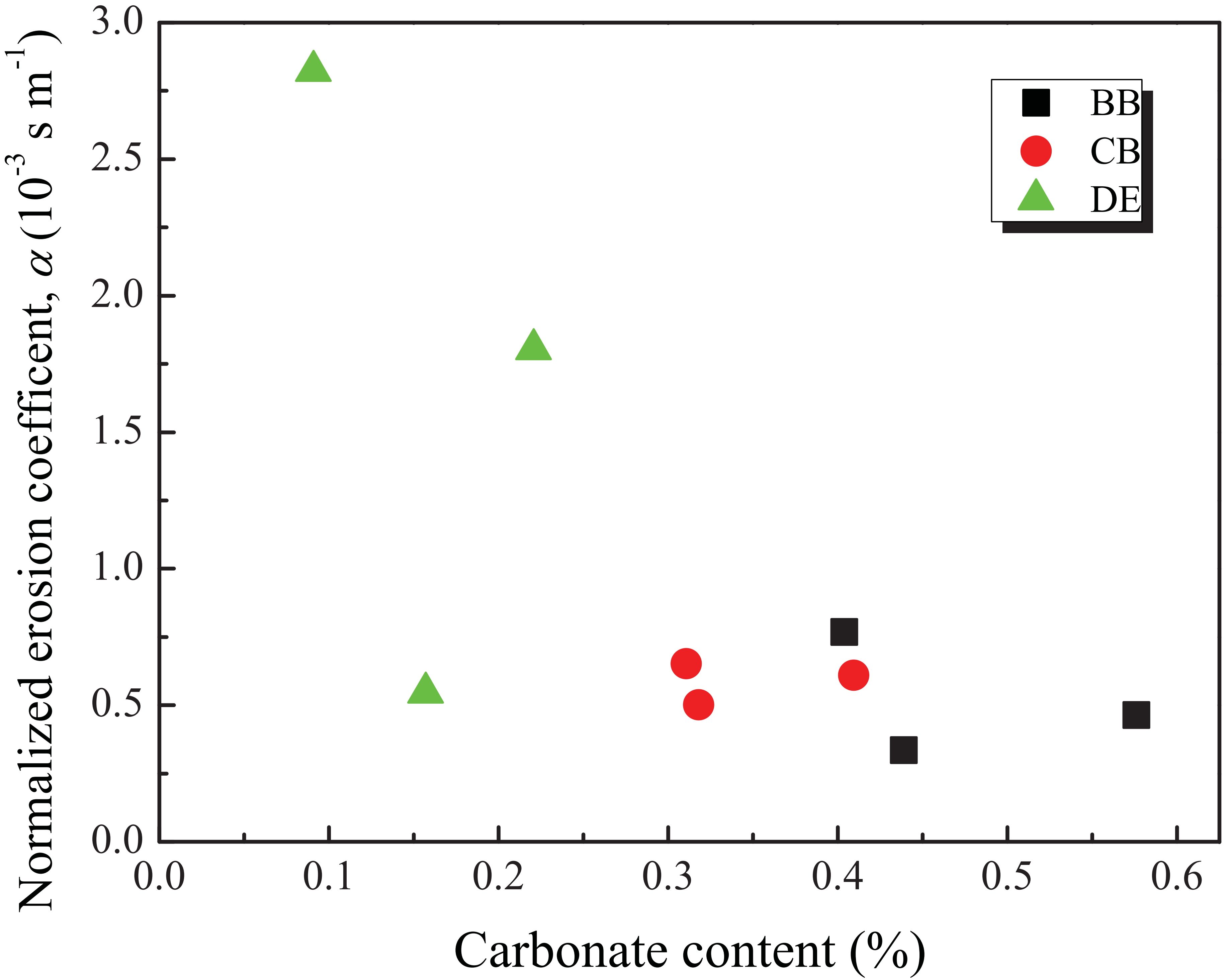

Normalized erosion coefficent, $\alpha$ ($10^{-3}$ s m$^{-1}$)
3.0
2.5
2.0
1.5
1.0
0.5
0.0
0.0
0.1
0.2
0.3
0.4
0.5
0.6
Carbonate content (%)
BB
CB
DE

Figure 15



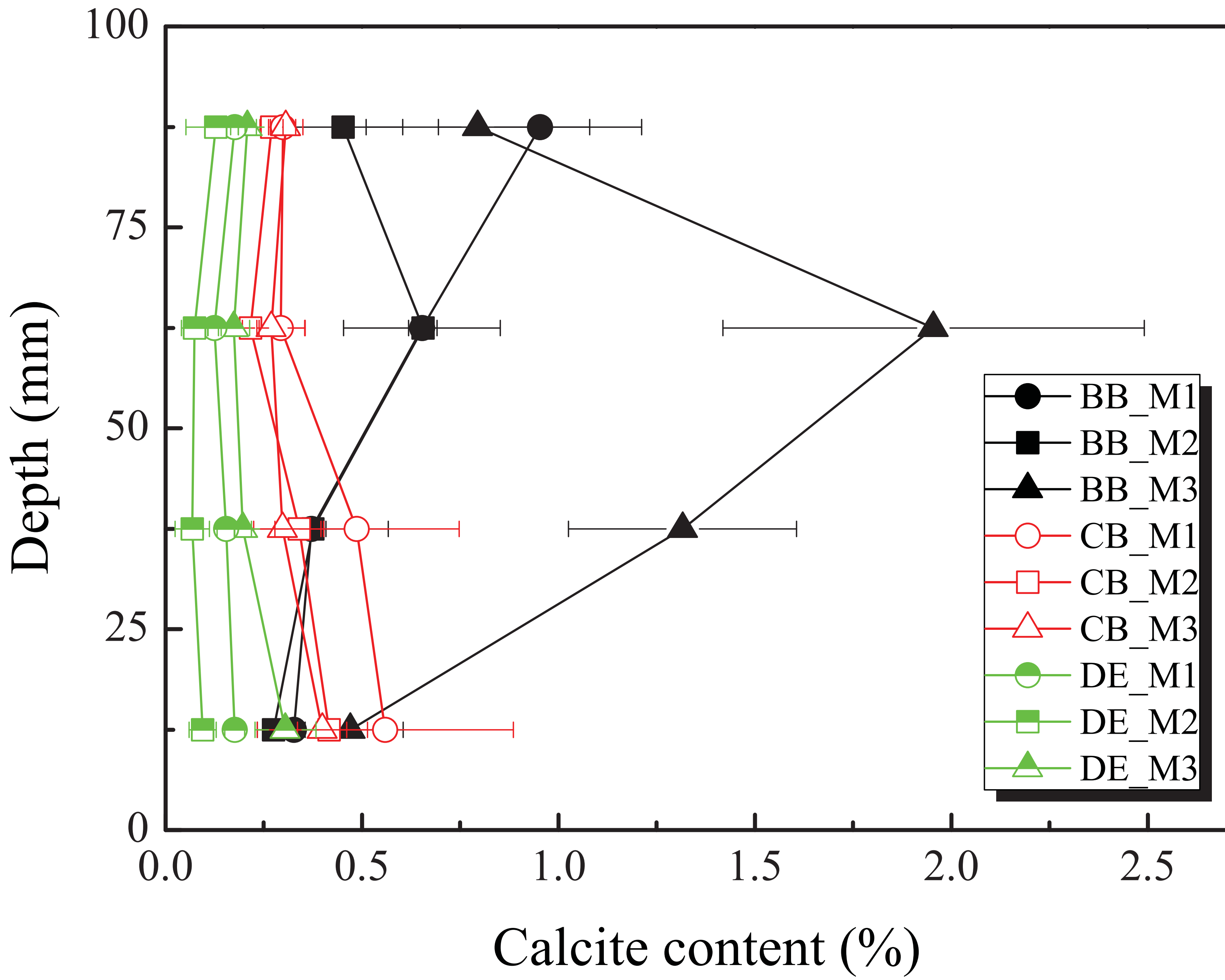

Depth (mm)
100
75
50
25
0
0.0
0.5
1.0
1.5
2.0
2.5
Calcite content (%)
BB_M1
BB_M2
BB_M3
CB_M1
CB_M2
CB_M3
DE_M1
DE_M2
DE_M3